MOLECULAR AND CELLULAR BIOLOGY, Feb. 2010, p. 640–656 Vol. 30, No. 3
0270-7306/10/$12.00 doi:10.1128/MCB.00882-09

Cyclin-Dependent Kinase 1-Mediated Bcl-x_L/Bcl-2 Phosphorylation Acts as a Functional Link Coupling Mitotic Arrest and Apoptosis[▽]

David T. Terrano, Meenakshi Upreti, and Timothy C. Chambers*

Department of Biochemistry and Molecular Biology, University of Arkansas for Medical Sciences, Little Rock, Arkansas 72205

Received 6 July 2009/Returned for modification 27 July 2009/Accepted 8 November 2009

Despite detailed knowledge of the components of the spindle assembly checkpoint, a molecular explanation of how cells die after prolonged spindle checkpoint activation, and thus how microtubule inhibitors and other antimitotic drugs ultimately elicit their lethal effects, has yet to emerge. Mitotically arrested cells typically display extensive phosphorylation of two key antiapoptotic proteins, Bcl-x_L and Bcl-2, and evidence suggests that phosphorylation disables their antiapoptotic activity. However, the responsible kinase has remained elusive. In this report, evidence is presented that cyclin-dependent kinase 1 (CDK1)/cyclin B catalyzes mitotic-arrest-induced Bcl-x_L/Bcl-2 phosphorylation. Furthermore, we show that CDK1 transiently and incompletely phosphorylates these proteins during normal mitosis. When mitosis is prolonged in the absence of microtubule inhibition, Bcl-x_L and Bcl-2 become highly phosphorylated. Transient overexpression of nondegradable cyclin B1 caused apoptotic death, which was blocked by a phosphodefective Bcl-x_L mutant but not by a phosphomimetic Bcl-x_L mutant, confirming Bcl-x_L as a key target of proapoptotic CDK1 signaling. These findings suggest a model whereby a switch in the duration of CDK1 activation, from transient during mitosis to sustained during mitotic arrest, dramatically increases the extent of Bcl-x_L/Bcl-2 phosphorylation, resulting in inactivation of their antiapoptotic function. Thus, phosphorylation of antiapoptotic Bcl-2 proteins acts as a sensor for CDK1 signal duration and as a functional link coupling mitotic arrest to apoptosis.

The cell division cycle is controlled by checkpoints, which ensure the fidelity of chromosome replication and segregation, as well as orderly progression through the cell cycle. If these critical events cannot be completed as scheduled, damaged cells, which might otherwise pose a threat to the organism as precancerous cells, are eliminated (16). The mitotic checkpoint, for example, produces a "prevent anaphase" signal until all the chromosomes are properly attached to kinetochores (22). Microtubule inhibitors (MTIs) and other antimitotic agents prolong the activation of this checkpoint, causing mitotic arrest, which culminates in cell death generally via intrinsic apoptosis, providing a rationale for the use of these agents as antitumor agents (20, 31). Intrinsic or mitochondrial apoptosis is regulated by the Bcl-2 family of proteins, which exhibit either pro- or antiapoptotic properties (17, 37). The BH3-only proapoptotic members act as essential initiators of intrinsic apoptosis, whereas the multidomain proapoptotic members, Bax and Bak, act as essential mediators of mitochondrial membrane permeability. Antiapoptotic Bcl-2 family members, including Bcl-x_L, Bcl-2, and Mcl-1, oppose apoptosis by binding to the proapoptotic members and neutralizing their activity.

The molecular mechanisms leading to cell death in response to spindle checkpoint activation have yet to be established. Indeed, how the spindle checkpoint couples to pathways regulating cell survival and death still represents an unresolved issue in cell biology (26, 35). Nonetheless, it seems reasonable to hypothesize that signals generated in response to prolonged mitotic arrest are eventually transduced to the apoptotic machinery. In this regard, it is striking that MTIs consistently induce the phosphorylation of two key antiapoptotic proteins, Bcl-2 and Bcl-x_L, whereas other apoptotic stimuli fail to do so (9, 13, 25). The results of studies with phosphodefective mutants of Bcl-2 and Bcl-x_L indicate that phosphorylation antagonizes their antiapoptotic function (2, 33, 36), but the precise mechanism(s) has yet to be fully clarified.

The identity of the kinase responsible for the extensive phosphorylation of Bcl-x_L and Bcl-2 that occurs in response to sustained spindle checkpoint activation is unresolved. Identification of this kinase is considered to be of critical importance, since it will provide insight into the molecular links between mitotic arrest and cell death, as well as the molecular mechanism of action of antimitotic drugs. Several candidates have been proposed, including Raf-1 (3), Jun N-terminal protein kinase (JNK) (2, 11, 36), protein kinase A (PKA) (32), cyclin-dependent kinase 1 (CDK1) (24), and mammalian target of rapamycin (mTOR) (4). In general, however, conclusions have been correlative or have been based on the use of kinase inhibitors tested under conditions that precluded mitotic arrest and thus indirectly blocked the effects of MTIs. Thus, strong experimental evidence supporting identification is lacking.

Here we present evidence that the CDK1/cyclin B kinase complex is responsible for mitotic arrest-induced Bcl-x_L/Bcl-2 phosphorylation. Furthermore, we show that CDK1 transiently and incompletely phosphorylates these proteins during normal mitosis. The findings suggest a model whereby a switch in the duration of CDK1 activation, from transient during mitosis to sustained during mitotic arrest, dramatically increases the extent of Bcl-x_L/Bcl-2 phosphorylation, resulting in inactivation of the antiapoptotic function of Bcl-x_L/Bcl-2. Thus, CDK1-mediated phosphorylation of antiapoptotic Bcl-2 proteins acts as a key link coupling mitotic arrest to apoptosis.

* Corresponding author. Mailing address: Department of Biochemistry and Molecular Biology, University of Arkansas for Medical Sciences, Mail Slot 516, 4301 W. Markham St., Little Rock, AR 72205-7199. Phone: (501) 686-5755. Fax: (501) 686-8169. E-mail: ChambersTimothyC@uams.edu.

▽ Published ahead of print on 16 November 2009.

MATERIALS AND METHODS

Materials. Antibodies against cyclin B1 (catalog no. sc-245), CDK1 (catalog no. sc-747), phospho-CDK1 (catalog no. sc-12341), JNK1 (catalog no. sc-474), and CDK2 (catalog no. sc-163) were purchased from Santa Cruz; antibodies against Bcl-x_L (catalog no. 2762), glyceraldehyde-3-phosphate dehydrogenase (GAPDH) (catalog no. 2118), and phospho-H3 histone (Ser10) (catalog no. 97015) were purchased from Cell Signaling; antibodies to cytochrome *c* (catalog no. 55643), cyclin A (catalog no. 14531A), and poly(ADP-ribose) polymerase (PARP) (catalog no. 556362) were purchased from Pharmingen; the antibody against phospho-H1 histone (catalog no. 06-597) was from Upstate; and the antibody against the oxidative phosphorylation (OX-PHOS) complex (catalog no. MS601) was from Molecular Probes. The fluorescein isothiocyanate (FITC)-conjugated donkey anti-rabbit IgG(H+L) (catalog no. 711-095-152) secondary antibody for immunofluorescence was purchased from Jackson ImmunoResearch. The MitoTracker Red CMSRos (catalog no. M7512) and 4′,6-diamidino-2-phenylindole (DAPI) (catalog no. D-3571) stains were purchased from Molecular Probes. The Cdc kinase subunit 1 (Cks-1) agarose conjugate (recombinant yeast $p13^{suc1}$ fused to glutathione *S*-transferase [GST] and covalently linked to Sepharose CL-4B) was purchased from Millipore. The FL62 peptide, with the amino acid sequence HLADSPAVNRRR, was synthesized at 95% purity by Genscript. [γ-^{32}P]ATP (250 μCi at 10 μCi/μl) was obtained from Perkin-Elmer. Calf thymus H1 histone was purchased from Calbiochem. Purified, activated JNK1 was obtained from Upstate Biotechnology, and purified active CDK1/cyclin A2 was purchased from SignalChem. Precast 16.5% acrylamide Tris/Tricine gels, in an 18-well format, were purchased from Bio-Rad. Vinblastine, Taxol, doxorubicin, and the molecular weight standard kit (MW-GF-200) for size exclusion chromatography, were obtained from Sigma. Thymidine, MG132, isopropyl-1-thio-β-D-galactopyranoside (IPTG), and (*R*)-roscovitine (Ros) were purchased from EMD Biosciences. Aminopurvalanol A and RO3306 were purchased from Axxora, and ZM447439 was from Tocris Bioscience. *Escherichia coli* strain BL21(DE3) was purchased from Novagen.

Cell culture and synchronization. The KB-3 human carcinoma cell line and mouse embryonic fibroblasts (MEFs) were maintained in monolayer culture at 37°C under 5% CO_2 in Dulbecco's modified Eagle's medium supplemented with 10% fetal bovine serum, 2 mM L-glutamine, 50 U/ml penicillin, and 50 μg/ml streptomycin. KB-3 cells were synchronized by a double thymidine block method as described previously (10). Briefly, cells (10^6) were incubated in a medium containing 2 mM thymidine for 16 h, released into a normal medium for 9 h, and then incubated for 16 h in a medium containing 2 mM thymidine. The time point of release into a fresh medium from this second block, with 98% of cells at the G_1/S boundary as determined by flow cytometry (10), was designated 0 h.

Preparation of whole-cell extracts and immunoblotting. To prepare whole-cell extracts for kinase reactions or size exclusion chromatography, KB-3 cells were harvested, washed, pelleted twice with cold phosphate-buffered saline (PBS) (5 min at 500 × *g*), and resuspended in lysis buffer (25 mM HEPES [pH 7.5], 300 mM NaCl, 0.1% Triton X-100, 1.5 mM $MgCl_2$, 0.2 mM EDTA, 0.5 mM dithiothreitol [DTT], EDTA-free complete protease inhibitor tablets [Roche], 20 μg/ml aprotinin, 50 μg/ml leupeptin, 10 μM pepstatin, 1 mM phenylmethylsulfonyl fluoride, 20 mM β-glycerophosphate, 1 mM Na_3VO_4, and 1 μM okadaic acid). The suspension was incubated for 15 min on ice with occasional mixing; insoluble material was removed by centrifugation (20 min at 100,000 × *g*); and the supernatant was retained as the whole-cell extract. The protein concentration was determined using the Bio-Rad protein assay. Immunoblotting was performed as described previously (11), and quantitation was carried out using ImageJ software.

Size exclusion FPLC. Whole-cell extracts were subjected to size exclusion chromatography on a Superdex-200 10/300 column by fast-pressure liquid chromatography (FPLC) (Amersham) using a flow rate of 0.2 ml/min in 50 mM Tris-HCl (pH 7.5)–300 mM NaCl. UV absorbance at 280 nm was monitored during elution, and fractions of 0.5 ml were collected in tubes containing Triton X-100 (final concentration, 0.1%), glycerol (final concentration, 5%), and protease and phosphatase inhibitors as described above. Molecular size standards were cytochrome *c* (12.4 kDa), carbonic anhydrase (29 kDa), albumin (66 kDa), alcohol dehydrogenase (150 kDa), β-amylase (200 kDa), and blue dextran (2,000 kDa).

Kinase assays. For assessment of FL62 kinase activity in column fractions, aliquots of 22 μl were incubated without or with FL62 (50 μg) at 30°C for 20 min in kinase reaction mixture (25 mM Tris-HCl [pH 7.5], 10 mM $MgCl_2$, 5 mM DTT, 1 μM ATP, and 1 μCi [γ-^{32}P]ATP). Reactions were stopped by addition of EDTA to 20 mM. For phosphorimage analysis, samples were boiled in sodium dodecyl sulfate (SDS) sample buffer, and a maximum of 10 μl (a minimum of 10 μg of FL62 for Coomassie blue visualization) was applied to 16.5% acrylamide Tris/Tricine high-resolution gels (referred to below as peptide-PAGE [polyacrylamide gel electrophoresis]). The gels were fixed in 5% glutaraldehyde overnight, washed extensively with distilled H_2O (dH_2O), and exposed to a phosphorimager screen. Controls and samples from drug-treated cells were always analyzed side by side with the same reagents and exposure times. Fractions from the void volume served as negative controls. Whole-cell extracts (5 μg protein) were assayed similarly with 10 μg FL62/reaction. For P81 phosphocellulose filter paper assays, the same incubation conditions were used except that the reaction mixtures contained 10 μg FL62 and 0.1 to 1 μCi [γ^{32}P]ATP. After incubation, reactions were stopped by addition of EDTA to 20 mM, acidified with 15% acetic acid, and spotted onto 2-cm-diameter P81 phosphocellulose filter discs (Fisher). Filters were washed with 75 mM H_3PO_4 (four times, with 500 ml each time) and air dried, and ^{32}P incorporation was measured by scintillation counting. *In vitro* reactions with active JNK1 contained 1 U of enzyme and either 15 μg FL62 or 1 μg GST–c-Jun in a kinase reaction mixture as described above. After 20 min at 30°C, reactions were terminated by the addition of EDTA to 20 mM, and reaction products were subjected to peptide-PAGE and phosphorimage analysis. An immune complex assay of CDK1/cyclin B was conducted using whole-cell extracts that were first precleared with mouse IgG for 30 min at 4°C, then incubated with mouse anti-cyclin B1 antibody for 2 h at 4°C, and finally incubated with mouse IgG agarose overnight at 4°C. The pellets were washed twice with lysis buffer and were subjected to kinase assays with FL62 (10 μg) or H1 histone (1 μg) as the substrate as described above. Separate immunoprecipitations were conducted for each reaction, and blank values were obtained by excluding the substrate.

Depletion of CDK with Cks-1. Whole-cell extracts (400 μg) were first incubated with the Cks-1 agarose conjugate (20 μl) for 3 h at 4°C and then pelleted, and the supernatant was incubated again with Cks-1 agarose (20 μl) for 3 h at 4°C. Extracts incubated for 6 h at 4°C without Cks-1 agarose served as controls. CDK-depleted and control extracts were subjected to kinase assays with 1 μg H1 histone or 10 μg FL62 for 20 min at 30°C in a kinase reaction mixture with 10 μM ATP and 1 μCi [γ-^{32}P]ATP. ^{32}P incorporation was determined by the phosphocellulose filter paper assay and scintillation counting as described above.

Flow cytometry. To determine cell cycle distribution, cells were collected by trypsinization, fixed in 70% ethanol, washed in PBS, resuspended in 1 ml of PBS containing 1 mg/ml RNase and 50 μg/ml propidium iodide, incubated for 20 min in the dark at room temperature, and analyzed by flow cytometry using a FACSCalibur instrument (Becton Dickinson, Mountain View, CA). The data were analyzed using the ModFit DNA analysis program (Verity Software House).

Preparation, phosphorylation, and mass spectrometry of His–Bcl-x_L–ΔC. Recombinant His–Bcl-x_L–ΔC, which has an amino-terminal histidine tag and lacks the carboxy-terminal transmembrane domain to enhance solubility, was prepared using standard methodology. Briefly, *E. coli* strain BL21(DE3) was transformed with plasmid pET29b-BclxL-ΔC, grown in 2× YT medium (16 g/liter tryptone, 10 g/liter yeast extract, 5 g/liter NaCl, pH adjusted to 7) (50 ml) containing 10 μg/ml kanamycin, and induced with 0.4 mM IPTG overnight at 30°C. Bacterial pellets were lysed on ice for 30 min in 5 ml of 50 mM phosphate buffer containing 0.3 M NaCl, 10 mM imidazole, 1 mg/ml lysozyme, and protease inhibitors. The bacterial lysate was sonicated, and cell debris was pelleted at 10,000 × *g* for 30 min. The cleared lysate was loaded onto a Qiagen nickel-nitrilotriacetic acid spin column, and after a wash, the His-tagged protein was eluted with 250 mM imidazole. His–Bcl-x_L–ΔC-containing fractions were pooled and dialyzed in Pierce Slide-A-Lyzer cassettes (Thermo Scientific) overnight at 4°C against a buffer containing 50 mM Tris-HCl (pH 7.5), 100 mM NaCl, 1 mM DTT, and 1 mM EDTA. Protein samples at a concentration of 1 mg/ml in 20% glycerol were stored at −70°C.

His–Bcl-x_L–ΔC (5 μg) was tested as a CDK1 substrate by incubation in kinase reaction mixture with [γ-^{32}P]ATP and up to 320 ng purified CDK1/cyclin A2 at 30°C for 20 min. Reaction products were subjected to SDS-PAGE, colloidal Coomassie staining, and phosphorimage analysis. To determine the site of phosphorylation, 5 μg His–Bcl-x_L–ΔC was incubated in kinase reaction mixture containing 1 μM nonradioactive ATP with or without 320 ng purified CDK1/cyclin A2, resolved by SDS-PAGE, and stained with colloidal Coomassie stain, and bands were excised from the gel. The proteins in each SDS-PAGE gel slice were reduced in 10 mM Tris(2-carboxyethyl) phosphine, alkylated in 50 mM iodoacetamide, and digested in-gel with AspN protease (Roche) for 4 h at 37°C. The resulting peptide products were separated by reverse-phase liquid chromatography using a C_{18} column resin (Phenomenex) on a nanoLC-2D HPLC system (Eksigent Technologies) and were analyzed by tandem mass spectrometry using an electrospray interface LTQ XL-Orbitrap mass spectrometer (Thermo). Protein identities were confirmed and phosphorylated amino acids identified by

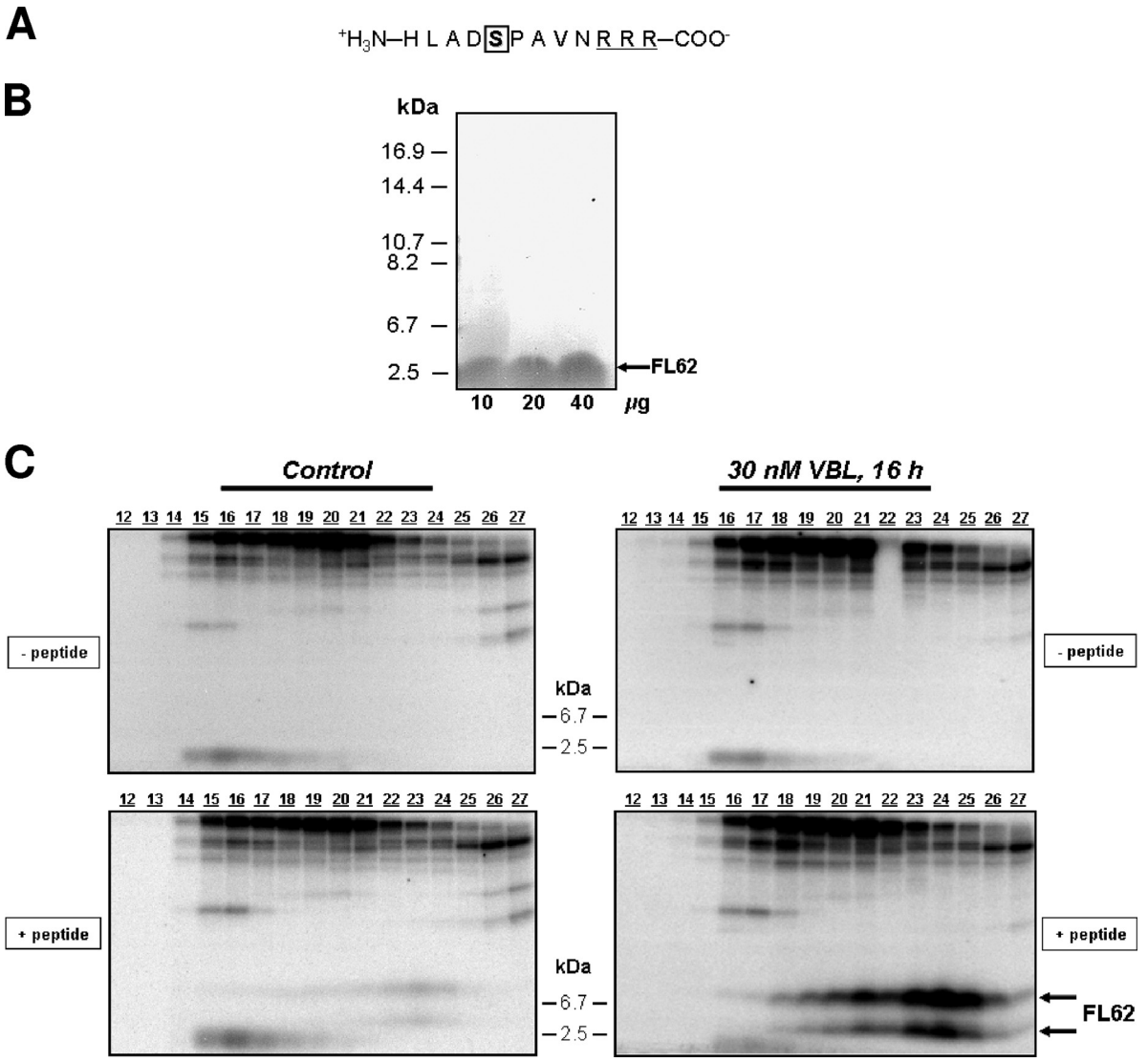

FIG. 1. Phosphorylation of a Bcl-x_L kinase peptide substrate. (A) Sequence of the FL62 peptide, representing amino acids 58 to 66 from the flexible loop (FL) of human Bcl-x_L with three C-terminal arginines. Ser62 is boxed. (B) Electrophoretic detection of FL62. The indicated amounts of FL62 in 10 μl were subjected to high-resolution 16.5% acrylamide Tris/Tricine SDS-PAGE and were visualized by Coomassie staining, as described in Materials and Methods. Molecular mass standards are indicated. (C) Phosphorylation of FL62. Protein extracts from untreated (control) (left) or vinblastine (VBL)-treated (right) KB-3 cells were size separated by FPLC using a Superdex-200 10/300 column. Fractions were incubated without (− peptide) or with (+ peptide) 50 μg of FL62 in the presence of [γ-^{32}P]ATP at 30°C for 20 min. Reaction mixtures were electrophoresed as for panel B, and gels were fixed overnight in 5% glutaraldehyde, washed extensively in dH_2O, and exposed to a phosphorimager screen, with each gel subjected to an equal exposure. Fraction numbers are given at the top of each gel, and the lower- and higher-molecular-weight forms of phosphorylated FL62 are indicated.

searching the IPI human database using the Mascot search engine (Matrix Sciences).

Subcellular fractionation and preparation of mitochondria. Cytosolic and mitochondrial fractions were prepared as described previously (8). Briefly, cells were harvested, washed in PBS, and resuspended in mitochondrial extraction buffer (MEB, comprising 10 mM HEPES [pH 7.5], 210 mM mannitol, 70 mM sucrose, and 1 mM EDTA, supplemented with protease and phosphatase inhibitors). Cells were lysed in a nitrogen cavitation bomb at 400 lb/in^2 for 5 min. This produced >95% lysis as determined by trypan blue staining. Cell debris and nuclei were removed by centrifugation (5 min at 2,000 × *g*) to produce the postnuclear supernatant. This was centrifuged at 13,000 × *g* for 15 min to pellet the total mitochondrial fraction, which was resuspended in 150 to 750 μl of MEB, depending on the amount of cells used. The supernatant was retained as the cytosol, which was further clarified at 100,000 × *g* for 1 h to remove insoluble material. To further purify mitochondria, the total mitochondrial fraction was layered over 1.2 M sucrose, which was layered over 1.6 M sucrose. Both sucrose solutions were prepared in 10 mM HEPES (pH 7.5), 1 mM EDTA, and 0.1% bovine serum albumin (BSA). The gradient was centrifuged at 27,000 rpm for 2 h in a Beckman SW28 rotor, and mitochondria were recovered at the 1.2 M–1.6 M sucrose interface and washed twice in MEB.

Immunofluorescence. Cells plated on glass coverslips were incubated with 30 nM MitoTracker Red for 20 min, which was replaced with fresh medium for 1.5 h and then changed again for 10 min. For vinblastine-treated samples, MitoTracker Red was added 2 h prior to harvest at 16 h of treatment. The remaining staining procedure was conducted at room temperature. The plates were washed twice with PBS, and cells were fixed and permeabilized with a 4% paraformaldehyde–0.18% Triton X-100 solution for 30 min. The cells were washed three times with PBS, blocked with a solution of 1% BSA in PBS for 30 min, washed three times with PBS, and then incubated with a polyclonal primary antibody against CDK1 (dilution, 1:50) or a monoclonal primary antibody against cyclin B

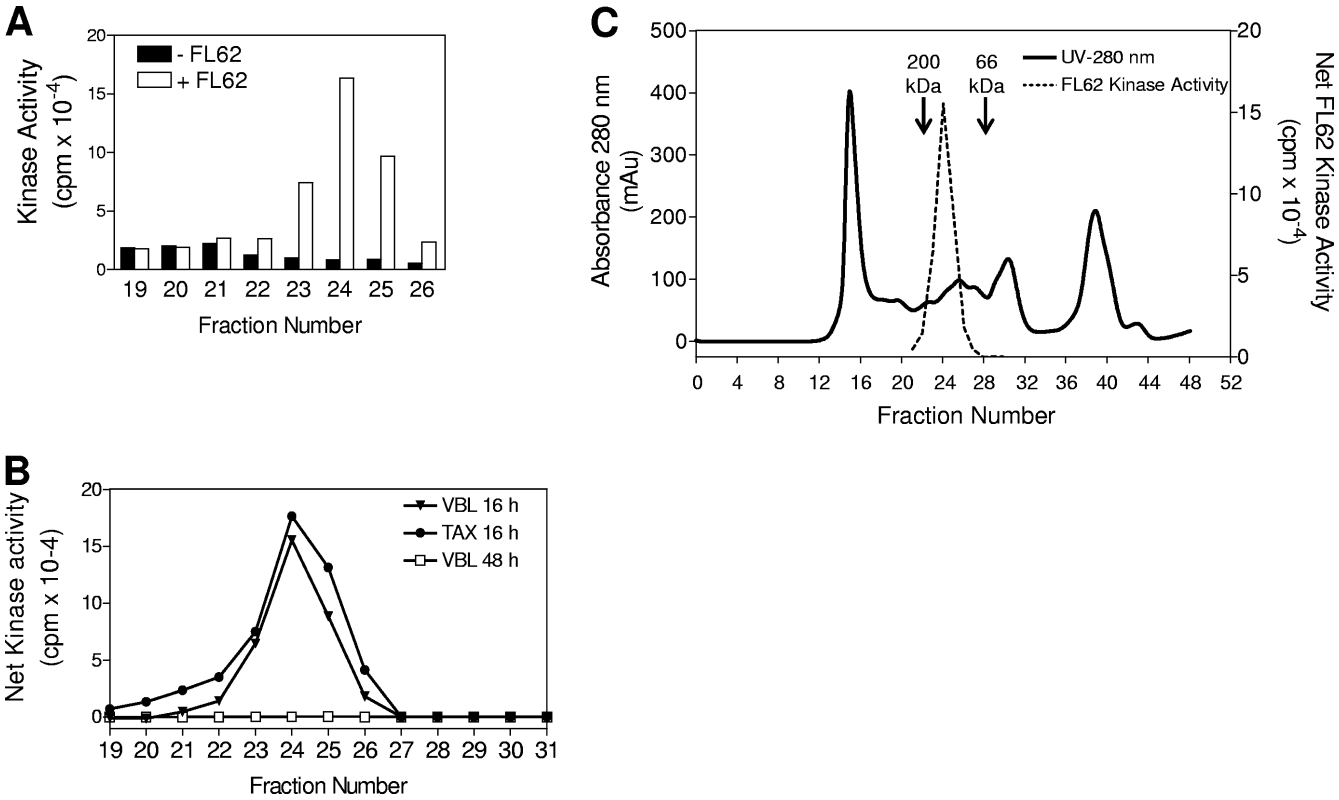

FIG. 2. Size exclusion chromatography of FL62 kinase. (A) Rapid phosphocellulose filter assay of FL62 kinase activity. The FPLC fractions used in the gel-based assay (Fig. 1C) were reassayed using a P81 filter assay. Fractions 19 to 26 were incubated with (open bars) or without (filled bars) 50 μg FL62 peptide in the presence of [γ-^{32}P]ATP at 30°C for 20 min. Reactions were stopped with 20 mM EDTA, and products were acidified with 15% acetic acid, spotted onto P81 filters, washed in 75 mM H_3PO_4, and dried. ^{32}P radioactivity was determined by scintillation counting. Data shown are representative of eight experiments. (B) FL62 kinase activity in vinblastine (VBL)- and Taxol (TAX)-treated cells. KB-3 cells were treated with 30 nM vinblastine for 16 h or 48 h, or with 30 nM Taxol for 16 h, and extracts were resolved by FPLC as for Fig. 1C. Net FL62 kinase activity was determined using the P81 filter paper assay as for panel A by subtracting the counts per minute of products of reactions without FL62 from those with FL62. (C) Molecular size estimation of FL62 kinase. The Superdex-200 FPLC absorbance profile at 280 nm (solid line) and the net FL62 kinase activity (dashed line) of the 16-h vinblastine extract (from panel B) are superimposed on the same graph. The elution positions of the 200-kDa and 66-kDa molecular size standards (β-amylase and albumin, respectively) are shown.

(dilution, 1:100) for 1 h. The cells were washed three times with PBS and were then incubated with an FITC-conjugated goat anti-rabbit secondary antibody (1:100) for 1 h. The cells were washed three times with PBS, and nuclei were stained with DAPI for 5 min, followed by three washes with PBS. Immunofluorescent protein (green), mitochondria (red), and nuclei (blue) were visualized using the 488-, 561-, and 405-nm laser lines, respectively, of a Zeiss LSM410 confocal microscope, and images were processed using Adobe Photoshop.

Transient transfections and apoptosis assays. KB-3 cells were transiently transfected with plasmid DNA using a combination of Lipofectamine and Lipofectamine Plus reagents (Invitrogen) according to the manufacturers' instructions. Cells were harvested 48 h after transfection for the apoptotic cell death assay and after 24 or 48 h for the detection of expressed proteins by immunoblotting. Apoptosis was determined using a cell death detection enzyme-linked immunosorbent assay (ELISA) kit (Roche Applied Science) as previously described (33). This is a quantitative photometric immunoassay for the determination of cytoplasmic histone-associated oligonucleosomes generated during apoptosis.

RESULTS

Validation of FL62 as a peptide substrate of the Bcl-x_L kinase. Recently, using protein purification and mass spectrometry, we identified the major vinblastine-induced phosphorylation site in Bcl-x_L as Ser62 (33), in the flexible-loop (FL) region between the BH3 and BH4 domains (37). We reasoned that a small peptide encompassing this site might act as a useful and specific substrate to facilitate identification of the vinblastine-activated Bcl-x_L kinase. A peptide that encompasses residues 58 to 66 of human Bcl-x_L, with three arginines added to the carboxy terminus to facilitate binding to phosphocellulose filters, was synthesized and designated FL62 (Fig. 1A). The 1.4-kDa peptide (molecular size confirmed by mass spectrometry) could be visualized by Coomassie staining after electrophoresis using peptide-PAGE, as described in Materials and Methods, where it migrated with an apparent molecular size of about 2.5 kDa (Fig. 1B). In order to test the peptide as a substrate, protein extracts from untreated and vinblastine-treated KB-3 cells were size fractionated by FPLC using a Superdex-200 column, and fractions were incubated under phosphorylation conditions with or without FL62. Samples were subjected to peptide-PAGE and phosphorimage analysis. Significant phosphorylation of FL62 was observed in extracts from vinblastine-treated cells and not in extracts from control cells, with peak activity at fraction 24 (Fig. 1C). Interestingly, the phosphorylated peptide migrated as two distinct bands on these gels (approximately 2.5 kDa and 7.5 kDa), with the

slower-migrating band containing most of the ^{32}P radioactivity (Fig. 1C) and the faster-migrating band corresponding to the bulk of the peptide as judged by Coomassie staining (data not shown). While the basis for this observation is unclear, it appears that phosphorylation may alter the conformation and/or SDS binding properties of the peptide or may promote the formation of FL62 oligomers.

Initial characterization of FL62 kinase and relationship to Bcl-x_L phosphorylation. In order to further characterize the FL62 kinase, and to avoid time-consuming assays involving gel electrophoresis that required prolonged fixation and extensive washing steps, a rapid P81 phosphocellulose filter disc method was tested. Reassay of the FPLC fractions confirmed that this method provided a robust and specific signal that precisely paralleled the peak of kinase activity observed in the peptide gels (Fig. 2A). Since Bcl-x_L phosphorylation is widely induced by MTIs (25), extracts from Taxol-treated cells were subjected to the same analysis. The same profile of FL62 kinase activity, again peaking at fraction 24, was observed (Fig. 2B). The absence of FL62 kinase activity in samples from cells treated with vinblastine for 48 h, a time point at which cellular Bcl-x_L has become dephosphorylated (9), also supported a correlation between FL62 kinase activity and the phosphorylation status of cellular Bcl-x_L (Fig. 2B). The profile of FL62 kinase activity from the Superdex column in relation to the protein absorbance profile and the elution of molecular mass standards provided an estimate of native molecular size in the range of 150 to 190 kDa (Fig. 2C).

To further document the drug specificity of FL62 kinase activation, cells were treated with doxorubicin, a DNA interchelator and topoisomerase inhibitor that does not induce mitotic arrest in KB-3 cells (9). Cell extracts were subjected to size exclusion FPLC and an FL62 kinase assay. FL62 phosphorylation was essentially undetectable in the extract from doxorubicin-treated cells (data available on request). Taken together, these results indicate that the FL62 kinase assay specifically detects the MTI-activated kinase responsible for Bcl-x_L phosphorylation *in vivo*.

Relationship to mitotic arrest. In order to facilitate the analysis of multiple samples, we tested whether FL62 kinase activity could be detected in whole-cell extracts. FL62 phosphorylation was readily observed when extracts derived from vinblastine-treated cells, but not untreated cells, were used as a source of kinase activity (Fig. 3A). Treatment of KB-3 cells with increasing concentrations of vinblastine indicated a dose-dependent response up to a maximum at 10 nM vinblastine (Fig. 3B, bar graph). The expression of cyclin B (Fig. 3B, dashed line in upper panel and Western blot in lower panel) and the percentage of cells with 4N DNA content (Fig. 3B) showed a dose dependency strikingly similar to that of the kinase activity which also closely paralleled the level of Bcl-x_L phosphorylation (Fig. 3B). These results suggest that the degree of activation of FL62 kinase is directly related to the extent of mitotic arrest and not to the vinblastine concentration *per se* and that kinase activity is also closely correlated with the phosphorylation of cellular Bcl-x_L.

FL62 kinase activation and Bcl-x_L phosphorylation during normal mitosis. Since FL62 kinase activity correlated with the degree of mitotic arrest, we explored whether the enzyme was also active during normal mitosis. Mitotic KB-3 cells were prepared by synchronizing them by the double thymidine block method, releasing them into medium, and harvesting 10 h later, a time that corresponds to M phase (9). Extracts were prepared and assayed for FL62 kinase activity. Mitotic cells showed a significant, 4-fold increase in FL62 kinase activity over asynchronous cells, while extracts from vinblastine-treated cells showed a 13-fold increase (Fig. 4A). Analysis of

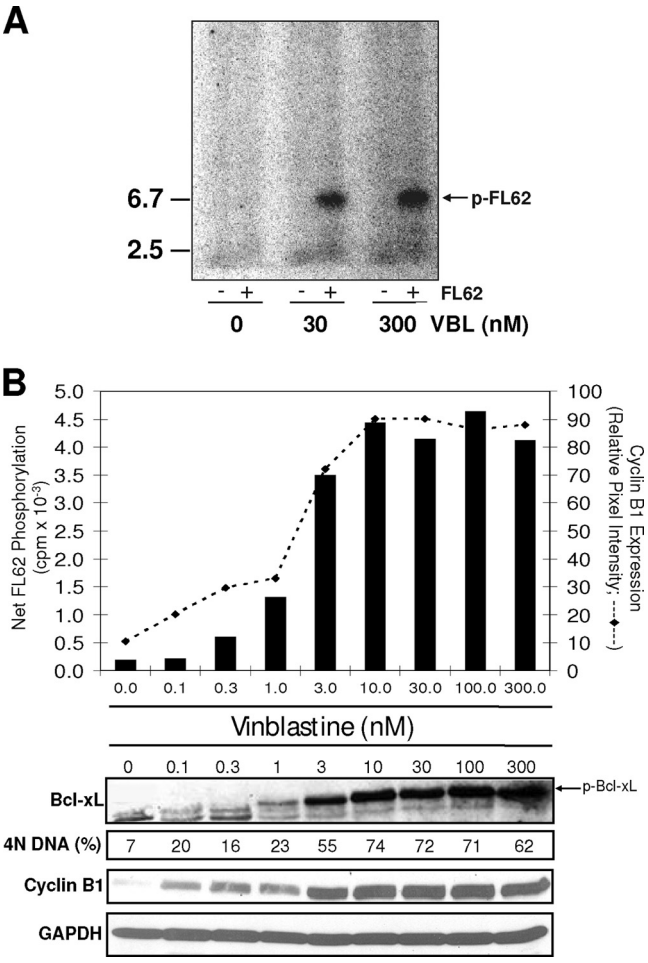

FIG. 3. The extent of FL62 kinase activity coincides with the degree of G_2/M arrest. (A) FL62 kinase activity in whole-cell extracts. KB-3 cells were either left untreated or treated with 30 or 100 nM vinblastine (VBL) for 16 h, and extracts were subjected to a FL62 kinase assay, peptide-PAGE, and phosphorimage analysis, as in Fig. 1C. The arrow indicates the migration position of phosphorylated FL62. (B) Quantitative relationship between FL62 kinase activity, G_2/M index, and cellular Bcl-x_L phosphorylation, induced by vinblastine. KB-3 cells were treated with vinblastine at the indicated concentrations for 16 h, and extracts were prepared for the determination of FL62 kinase activity (bar graph) (upper panel) and for immunoblotting for the indicated proteins (lower panels). FL62 kinase activity was determined by the P81 phosphocellulose assay, by subtracting the level of ^{32}P incorporation in the products of reactions without FL62 from those with FL62 to calculate net FL62 phosphorylation. Reactions were performed in triplicate, and the average values were plotted. The dashed line represents cyclin B expression, determined by densitometry from the blot shown in the lower panel, as described in Materials and Methods. The percentage of cells with 4N DNA was determined by propidium iodide staining and flow cytometry, as described in Materials and Methods.

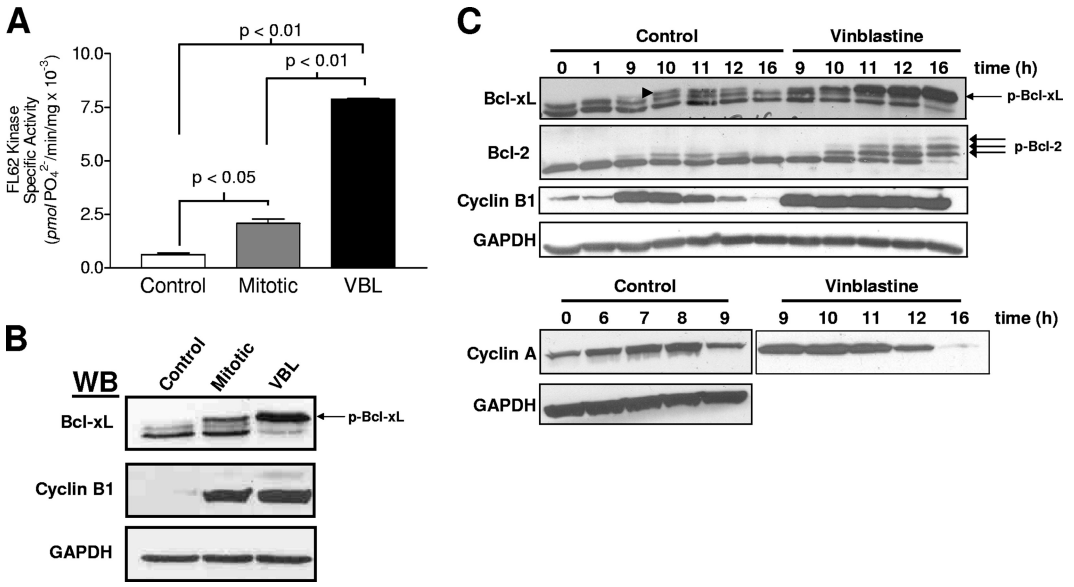

FIG. 4. Partial Bcl-x_L/Bcl-2 phosphorylation and FL62 kinase activation during normal mitosis. (A) FL62 kinase activity during normal mitosis. Extracts were prepared from untreated asynchronous KB-3 cells (control), KB-3 cells synchronized in mitosis (mitotic) by a double thymidine block with harvest 10 h after release, or asynchronous KB-3 cells treated with 30 nM vinblastine (VBL) for 16 h. Extracts were incubated without or with FL62 in a kinase reaction mixture and were analyzed by the P81 filter assay. The specific activity of FL62 kinase (picomoles of phosphate incorporated into FL62 per minute per milligram of cell extract) is shown for each condition. Results are means ± standard deviations ($n = 6$). (B) Phosphorylation of cellular Bcl-x_L during normal mitosis. Extracts from untreated, mitotic, or vinblastine-treated cells (from panel A) were subjected to immunoblotting for Bcl-x_L and cyclin B. GAPDH was used as a loading control. (C) Bcl-x_L phosphorylation dynamics during the normal cell cycle and following vinblastine treatment. KB-3 cells were synchronized by a double thymidine block. Cells were either left untreated (control) or treated with 30 nM vinblastine 1 h after release, and they were harvested at the indicated times after release. Extracts were subjected to immunoblotting for Bcl-x_L, Bcl-2, cyclin B, cyclin A, or GAPDH, as indicated. Phosphorylated Bcl-x_L is indicated by an arrow in vinblastine-treated samples and by an arrowhead in control samples (9- to 12-h time points).

Bcl-x_L from the same samples showed that while control cells and vinblastine-treated cells had unphosphorylated and fully phosphorylated Bcl-x_L, respectively, Bcl-x_L from mitotic cells was intermediate, with roughly equal proportions of unphosphorylated (lowest band) and phosphorylated (uppermost band) Bcl-x_L (Fig. 4B). Thus, in mitotic cells, an incomplete level of Bcl-x_L phosphorylation was observed in parallel with relatively modest activation of FL62 kinase.

Next, a more comprehensive experiment was conducted. Several flasks of cells were synchronized at the G_1/S boundary; different sets were released into medium containing either the vehicle or vinblastine; and cells were harvested at defined time points thereafter. During the 9- to 12-h period postrelease, which comprised the time from late G_2 phase into mitosis and the beginning of the next G_1 phase (10), Bcl-x_L in the control set underwent partial and transient phosphorylation (Fig. 4C, arrowhead). This occurred in close concert with cyclin B expression levels and did not correlate with cyclin A expression, which peaked earlier, at 7 to 8 h postrelease (Fig. 4C). When released in the presence of vinblastine, Bcl-x_L underwent complete and sustained phosphorylation, and this again occurred in concert with sustained cyclin B expression and was unrelated to cyclin A expression, which diminished to near-undetectable levels by 16 h (Fig. 4C). Bcl-2 showed essentially the same profile of phosphorylation, with partial and transient phosphorylation during normal mitosis versus sustained (and in this case, multisite) phosphorylation following vinblastine treatment (Fig. 4C). Thus, a vinblastine-induced mitotic block alters the temporal kinetics and extent of Bcl-x_L/Bcl-2 phosphorylation, from transient and incomplete during normal mitosis to sustained and complete, and this closely parallels cyclin B but not cyclin A expression.

FL62 kinase corresponds to CDK1/cyclin B and is distinct from JNK. The temporal and quantitative relationship between FL62 kinase activity and Bcl-x_L/Bcl-2 phosphorylation during mitosis and mitotic arrest suggested that CDK1, and more specifically CDK1/cyclin B, may be the FL62 kinase. Several experiments were conducted to explore this relationship further. First, FL62 kinase activity was found to coelute from the Superdex-200 column with active CDK1/cyclin B complexes (data available on request). In addition, FL62 was an excellent *in vitro* CDK1 substrate, comparable to histone H1 (Table 1). To demonstrate more conclusively that FL62 kinase was a CDK, the Cks-1 protein $p13^{suc1}$ from yeast conjugated to agarose, which directly binds CDKs (14), was used to deplete CDKs from whole-cell extracts of vinblastine-treated KB-3 cells. Kinase activities using both FL62 and H1 histone as substrates were measured in the original extract and following depletion. FL62 and H1 kinase activities decreased similarly, by more than 50%, following CDK depletion (Fig. 5A). Immunoblotting showed that CDK1 and cyclin B were present in the Cks-1 pellet, and furthermore, these proteins were roughly equally distributed between the pellet and the supernatant following depletion (Fig. 5B), quantitatively consistent with the depletion of kinase activity. JNK1, on the other hand, was retained in the supernatant and was undetectable in the Cks-1

TABLE 1. *In vitro* phosphorylation of FL62 by CDK1[a]

Assay condition	^{32}P incorporation (cpm)		
	Assay values	Avg	Net (%)
No substrate	24,456, 25,131	24,974	0
Histone H1	644,693, 659,460, 658,373	654,175	629,382 (100)
FL62	809,686, 813,972, 802,739	808,799	784,006 (125)

[a] An active CDK1/cyclin A2 complex was incubated alone or with 5 μg histone H1 or 1 μg FL62 in a kinase reaction mixture for 20 min at 30°C with 1 μM ATP and 1 μCi [γ-^{32}P]ATP. Reactions were conducted in triplicate, and ^{32}P incorporation was determined by a P81 phosphocellulose paper binding assay.

pellet (Fig. 5B), demonstrating the specificity of Cks-1 and excluding JNK as the FL62 kinase. The conclusion that FL62 kinase is distinct from JNK was supported by probing Superdex-200 FPLC fractions for JNK1 and JNK2 immunoreactivity. JNK1 was present mostly in fractions 30 to 32, with a peak at fraction 31, while JNK2 eluted earlier, in fractions 28 to 30, with a peak at fraction 29 (Fig. 5C), in contrast to FL62 kinase activity, which was detectable mainly in fractions 23 to 25 (Fig. 1C). FL62 was also tested as a substrate for active recombinant JNK1, and no detectable phosphorylation was observed, whereas an authentic substrate, GST–c-Jun, was readily phosphorylated (Fig. 5D). Thus, FL62 kinase is distinct from JNK isozymes, and FL62 is an ineffective substrate for JNK.

To further confirm that the FL62 kinase corresponded to CDK1/cyclin B, cyclin B was immunoprecipitated, and H1 histone and FL62 kinase activities were measured in the immunoprecipitated material. As shown in Fig. 6A, mitotic extracts demonstrated significantly higher CDK1/cyclin B kinase activity toward both substrates than control extracts, and CDK1/cyclin B kinase activity was increased further in extracts from vinblastine-treated cells. While maximum CDK1 activity may be expected both in mitotic extracts and in extracts from mitotically arrested cells, this was not observed; we consistently found greater CDK1 activity with either substrate in mitotically arrested cells (Fig. 4A and 6A; also data not shown). This observation may reflect the fact that untreated cells harvested at 10 h postrelease may differ from one another, to some degree, with respect to proximity to M phase. In support of this possibility, CDK1 activation appeared more complete in extracts from vinblastine-treated cells than in mitotic extracts, as judged by CDK1 gel mobility, where the faster-migrating species represents the dephosphorylated, catalytically active form of the kinase (Fig. 6B).

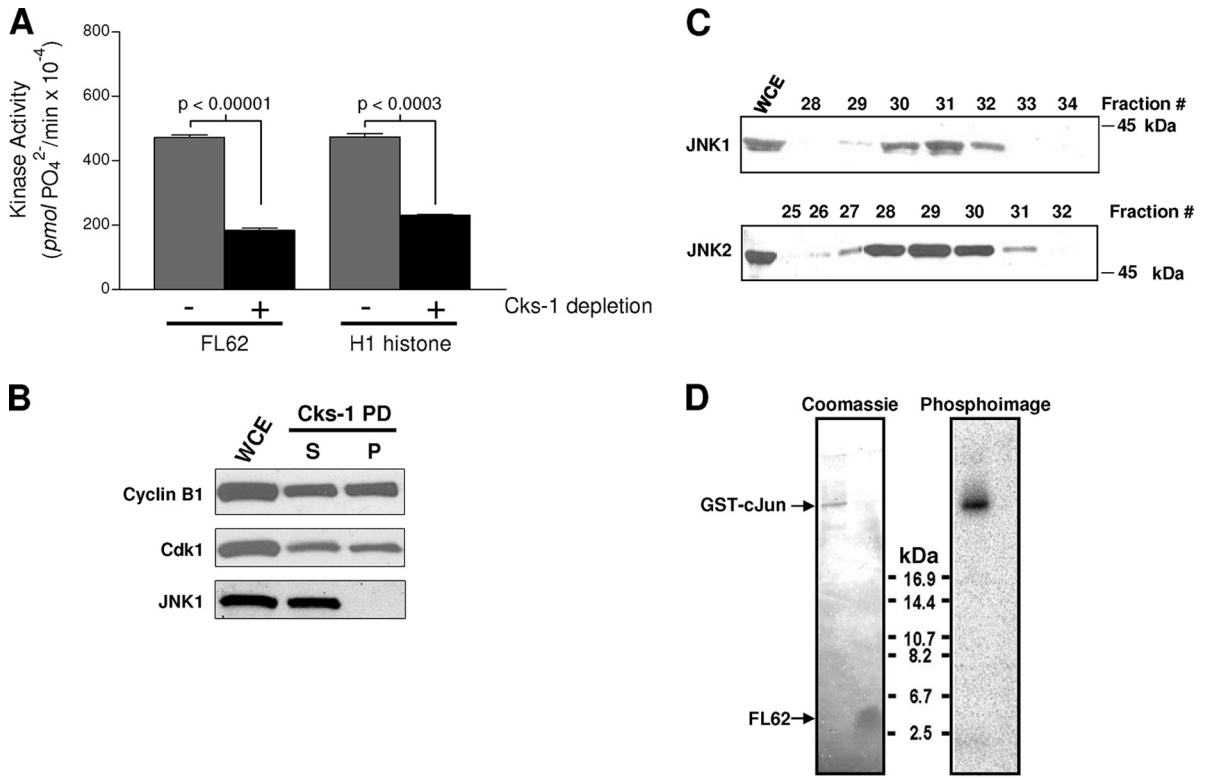

FIG. 5. FL62 kinase is a cyclin-dependent kinase and is distinct from JNK. A whole-cell extract (WCE) of KB-3 cells treated with vinblastine (30 nM, 16 h) was incubated with Cks-1-conjugated agarose beads. (A) The original extract and that depleted with Cks-1 were incubated with FL62 (10 μg) or H1 histone (1 μg) for 20 min at 30°C in a kinase reaction mixture containing 10 μM ATP and 1 μCi [γ-^{32}P]ATP, and phosphorylation was determined using the P81 filter paper assay. Phosphorylation in the absence of a substrate was subtracted. Data are means ± standard deviations (n = 3). (B) The WCE, as well as the supernatant (S) and the pellet (P) from the Cks-1 pulldown (Cks-1 PD) shown in panel A (15% of the total sample in each case), was immunoblotted for the indicated proteins. (C) Size-separated FPLC fractions from KB-3 cells treated with vinblastine (30 nM, 16 h) were immunoblotted for JNK1 and JNK2. A WCE from the same cells was also analyzed. The migration of a 45-kDa standard is shown. (D) FL62 was incubated with purified active JNK1 in a kinase reaction, subjected to peptide-PAGE, and analyzed by Coomassie blue staining and a phosphorimager. GST–c-Jun was used as a positive control, and the migration positions of GST–c-Jun and FL62 are indicated.

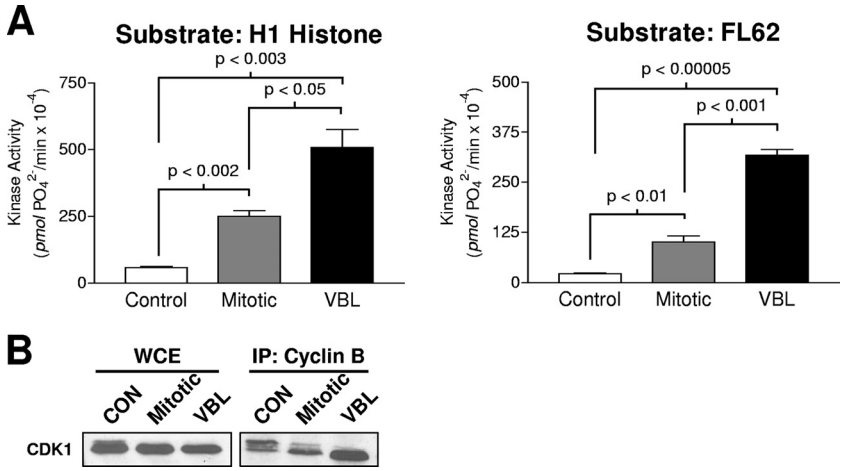

FIG. 6. Phosphorylation of FL62 by immunoprecipitated CDK1/cyclin B. (A) Extracts were prepared from untreated asynchronous KB-3 cells (control), untreated synchronized cells harvested 10 h after release (mitotic), and asynchronous cells treated with 30 nM vinblastine for 16 h (VBL). Cyclin B1 was immunoprecipitated, and after a wash, the immunoprecipitates were subjected to FL62 or H1 histone kinase assays, as described in Materials and Methods. Data are means ± standard deviations ($n = 3$), with blank (no-substrate) values subtracted; *P* values are shown. (B) Whole-cell extracts (WCE) and immunoprecipitates were immunoblotted for CDK1. CON, control.

CDK inhibitors inhibit vinblastine-induced Bcl-x_L/Bcl-2 phosphorylation. Next, we tested whether vinblastine-induced phosphorylation of cellular Bcl-x_L and Bcl-2 occurred in a CDK1-dependent manner. For this purpose, several validated CDK inhibitors were selected, including Ros (19), purvalanol A (PA) (27), and RO-3306 (RO) (34). Because these compounds inhibit CDKs in general, it was reasoned that they may delay or block cell cycle progression to M phase and thus prevent Bcl-x_L/Bcl-2 phosphorylation indirectly. To avoid this potential problem, cells were synchronized by a double thymidine block and were treated with vinblastine 1 h after release from G_1/S phase, and the CDK inhibitors were added later, for a short duration, at several time points corresponding to late G_2 and M phase. Specifically, the CDK inhibitors, or the dimethyl sulfoxide (DMSO) vehicle, were added for 2 h at 10, 11, or 12 h following G_1/S release in the presence of vinblastine. This experimental strategy is schematized in Fig. 7A. Extracts were made and subjected to immunoblotting for Bcl-x_L, Bcl-2, cyclin B1, phospho-H1 histone (a marker of CDK1 activity), and phospho-H3 histone (a marker of mitosis). The immunoblot data are shown in Fig. 7B. Lane 1 shows the baseline, that is, blots performed on cell extracts at the time of the second release (0 h). Comparison of lanes 2 and 6 in Fig. 7B shows that vinblastine induced a marked increase in Bcl-x_L and Bcl-2 phosphorylation during the interval from 10 h to 12 h postrelease, as expected. In the presence of CDK inhibitors during this interval, Bcl-x_L/Bcl-2 phosphorylation was strongly inhibited (Fig. 7B, compare lanes 3, 4, and 5 with lane 6). H1 histone phosphorylation showed a similar inhibitory profile. Blotting for phospho-H3 histone showed that levels increased from 10 to 12 h (Fig. 7B, compare lanes 2 and 6), and that Ros or PA treatment during this interval maintained phospho-H3 histone at the initial (10-h) levels. However, after RO treatment, phospho-H3 histone levels were markedly diminished (Fig. 7B, compare lanes 2 and 5), suggesting that RO may have been causing mitotic slippage. Examination of the data obtained at 11 to 13 h after G_1/S release in the presence of vinblastine (Fig. 7B, lanes 7 to 11) was additionally revealing. During this interval, Bcl-x_L/Bcl-2 phosphorylation increased markedly (Fig. 7B, compare lanes 7 and 11), and Ros blocked this increase without affecting the phospho-H3 histone level and hence without causing mitotic exit. In contrast, PA and RO caused a reversal of Bcl-x_L/Bcl-2 phosphorylation and, in concert, appeared to promote mitotic exit, as judged by reductions in the levels of phospho-H3 histone and cyclin B (Fig. 7B, compare lanes 8, 9, and 10 with lane 11). Examination of the data obtained during the interval from 12 to 14 h showed that Bcl-x_L/Bcl-2 phosphorylation was close to maximum at 12 h and that Ros blocked the modest increase occurring over the next 2 h, while PA and RO again caused a reversal of Bcl-x_L/Bcl-2 phosphorylation by inducing mitotic exit (Fig. 7B, lanes 12 to 16).

Inhibition of Bcl-x_L/Bcl-2 phosphorylation is not a consequence of mitotic slippage. The results with the CDK1 inhibitors shown in Fig. 7B strongly suggested that the reversal of Bcl-x_L/Bcl-2 phosphorylation caused by RO and PA, coinciding with a loss of H3 histone phosphorylation and a decrease in cyclin B1 expression, was a consequence of mitotic slippage. Furthermore, previous work has indicated that RO, the most potent of the three CDK1 inhibitors *in vitro* (50% inhibitory concentrations [IC_{50}], 20 nM for RO, 33 nM for PA, and 650 nM for Ros), can cause mitotic slippage (34). Dephosphorylation of Bcl-x_L and Bcl-2 as a result of mitotic slippage complicates the interpretation of the effect of the CDK inhibitors on the phosphorylation of these proteins. To clarify this issue, the proteasome inhibitor MG132 was used to prevent cyclin B degradation and subsequent mitotic slippage (30). KB-3 cells were synchronized, treated with vinblastine, and treated with the CDK1 inhibitors in the presence or absence of MG132 pretreatment (Fig. 7C). The increase in Bcl-x_L/Bcl-2 phosphorylation occurring during the interval from 11 to 13 h postrelease (Fig. 7C, compare lanes 1 and 8) was blocked in the presence of Ros (lane 2), and this blockage was unaffected by the proteasome inhibitor (lane 3). Also consistent with the

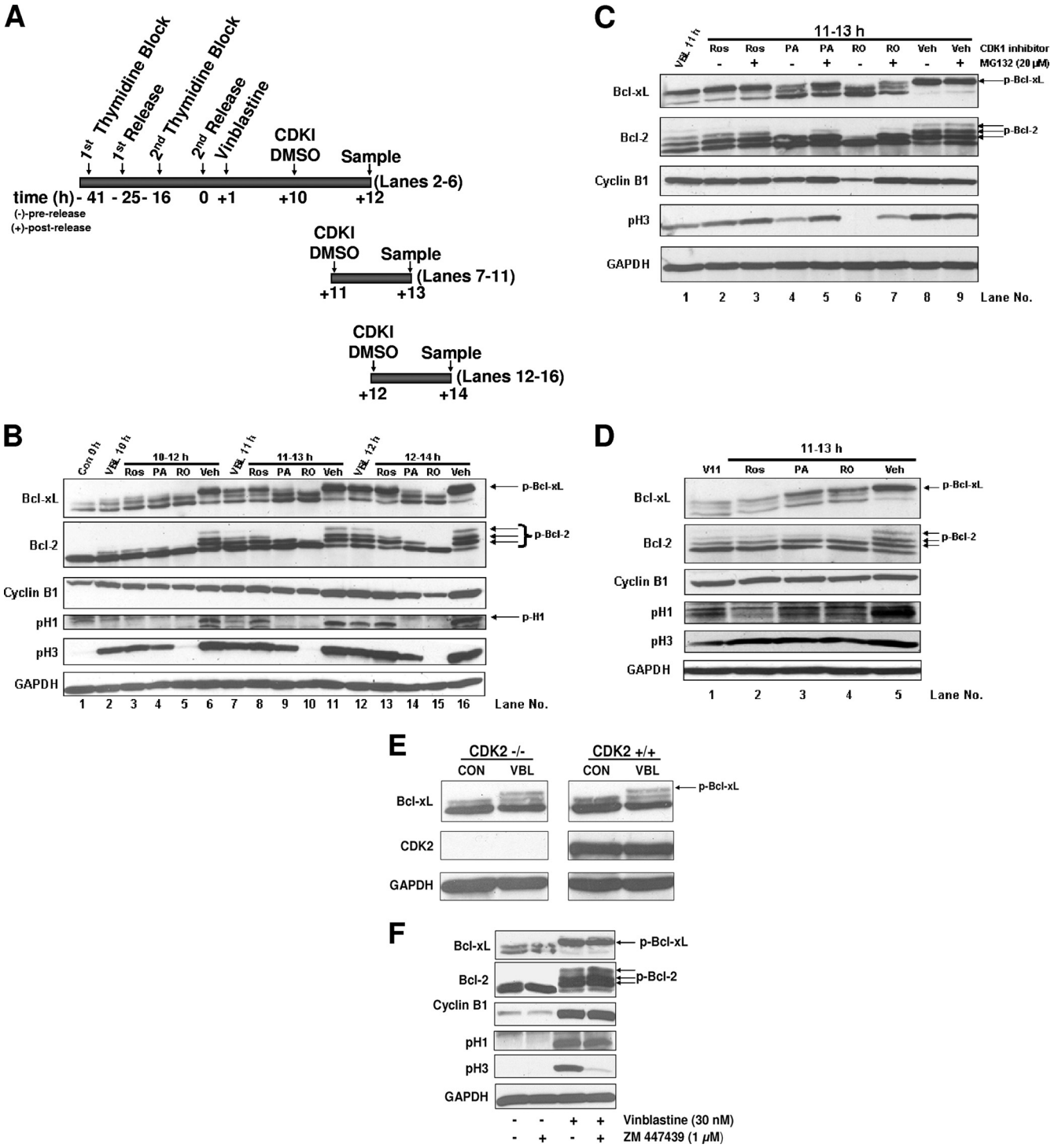

FIG. 7. Multiple CDK inhibitors inhibit vinblastine-induced Bcl-x_L/Bcl-2 phosphorylation. (A) Experimental design. The timing of events for cell synchrony by a double thymidine block and cell cycle-specific timing of CDK1 inhibition following vinblastine treatment are shown. Lane numbers refer to panel B. (B) CDK inhibitors block Bcl-x_L/Bcl-2 phosphorylation during mitotic arrest. KB-3 cells were synchronized at the G_1/S boundary by a double thymidine block and were treated with 30 nM vinblastine (VBL) 1 h after release. Cells were harvested at 10 h, 11 h, 12 h, and 14 h after release or were treated with 25 μM Ros, 10 μM PA, 10 μM RO, or the DMSO vehicle (Veh) for 2 h during the periods from 10 to 12 h, 11 to 13 h, and 12 to 14 h after release. An untreated dish of cells harvested immediately after release from the double thymidine block (Con, 0 h) was included as a control. Arrows indicate phosphorylated forms of Bcl-x_L, Bcl-2, or phospho-H1 histone. Whole-cell extracts were prepared and immunoblotted for the indicated proteins. GAPDH was used as a loading control. (C) CDK inhibitors maintain inhibition of Bcl-x_L phosphorylation when the proteasome is inhibited. KB-3 cells were synchronized at the G_1/S boundary by a double thymidine block and were treated with 30 nM VBL 1 h after release. Cells were harvested 11 h after release or were incubated for 2 h (i.e., from 11 to 13 h after release) with 25 μM Ros, 10 μM PA, 10 μM RO, or DMSO in the presence or absence of the proteasome inhibitor MG132 (20 μM). MG132 was added 20 min prior to the addition of the CDK inhibitors. Immunoblotting for the indicated proteins was performed. Arrows indicate phosphorylated (p) forms. (D) The CDK inhibitors PA and RO block Bcl-x_L phosphorylation at concentrations that do not cause mitotic slippage. KB-3 cells were synchronized at the G_1/S

earlier results shown in Fig. 7B, PA and RO reversed vinblastine-induced Bcl-x_L/Bcl-2 phosphorylation to some degree (Fig. 7C, lanes 4 and 6). However, in the presence of MG132, dephosphorylation was rescued (Fig. 7C, lanes 5 and 7), and the phosphorylation level of Bcl-x_L/Bcl-2 was maintained at approximately the original control level (Fig. 7C, lane 1), similar to the level of inhibition by Ros alone (lane 2). In addition, MG132 rescued the PA- and RO-induced loss of cyclin B and phospho-H3 histone, confirming that the proteasome inhibitor prevented mitotic slippage induced by these CDK inhibitors. Further, H1 histone phosphorylation was still susceptible to inhibition by the CDK inhibitors in the presence of MG132. Overall, these results show that inhibiting CDK1 activity while the cells are still mitotically arrested inhibits Bcl-x_L/Bcl-2 phosphorylation.

The concentrations of PA and RO (10 μM) used in the cell culture experiments described above are 300- and 500-fold greater, respectively, than their *in vitro* IC_{50}s for CDK1 (33 and 20 nM, respectively). Because Ros, when used at a concentration~30-fold higher than its IC_{50} for CDK1 (650 nM), effectively inhibited CDK1 without causing mitotic slippage, we tested whether lower concentrations of PA and RO would achieve a similar outcome. As shown in Fig. 7D, this was indeed the case. PA and RO used at 1 μM strongly inhibited vinblastine-induced Bcl-x_L/Bcl-2 phosphorylation, as well as H1 histone phosphorylation, occurring at 11 to 13 h postrelease, under conditions where mitotic slippage was prevented, as shown by the maintenance of cyclin B and phospho-H3 histone levels. Collectively, the results of Fig. 7A through D provide compelling evidence that vinblastine-induced Bcl-x_L/Bcl-2 phosphorylation is mediated via a CDK1-dependent pathway.

Vinblastine induces Bcl-x_L phosphorylation in CDK2-null cells. The temporal kinetics of vinblastine-induced Bcl-x_L phosphorylation coincided with CDK1/cyclin B activation. As further support for this identification, and to exclude other CDKs, wild-type ($CDK^{+/+}$) and CDK2-null ($CDK2^{-/-}$) primary MEFs were treated with vinblastine, and Bcl-x_L phosphorylation was analyzed. After 8 h of vinblastine treatment, a time point found to be optimal, $CDK2^{+/+}$ and $CDK2^{-/-}$ MEFs displayed comparable levels of Bcl-x_L phosphorylation (Fig. 7E). In contrast to the situation in KB-3 cells, however, phosphorylation was incomplete, with only a partial shift of the fastest-migrating band (unphosphorylated Bcl-x_L) to the slowest-moving band (phosphorylated Bcl-x_L), estimated to be 15% of total Bcl-x_L after quantitation. This partial response closely reflected the cellular response, in that only 10 to 15% of MEFs in the population appeared to be affected by the drug, showing rounding and loss of adherence, whereas the majority were morphologically normal. Such nonresponsiveness may be due to the fact that primary fibroblasts have a tendency to become quiescent in culture and thus refractory to cell cycle inhibitors. Thus, while the extent of Bcl-x_L phosphorylation appeared to be cell type specific, the highly similar responses of $CDK2^{+/+}$ and $CDK2^{-/-}$ MEFs indicate that CDK2 is not required for vinblastine-induced Bcl-x_L phosphorylation.

Inhibition of aurora B does not affect vinblastine-induced Bcl-x_L/Bcl-2 phosphorylation. The data presented above show that Bcl-x_L/Bcl-2 phosphorylation can be inhibited by CDK inhibitors in mitotically arrested cells where H3 histone phosphorylation is maintained. Mitotic H3 histone phosphorylation at Ser10 is catalyzed by the Ser/Thr spindle checkpoint aurora B kinase (15). To further determine whether Bcl-x_L/Bcl-2 phosphorylation and H3 histone phosphorylation are independent aspects of mitotic checkpoint signaling, and to test aurora B as a candidate Bcl-x_L kinase, a small-molecule inhibitor of aurora B, ZM447439, was utilized. Cells were synchronized by a double thymidine block and were treated with a vehicle or vinblastine at 1 h postrelease; then the vehicle or ZM447439 was added at 9 h postrelease, and cells were harvested at 16 h postrelease. As shown in Fig. 7F, ZM447439 inhibited H3 histone phosphorylation without affecting the phosphorylation of Bcl-x_L, Bcl-2, or H1 histone, or the expression of cyclin B. This experiment argues against aurora B as a candidate Bcl-x_L kinase and shows that under conditions where H3 histone phosphorylation is inhibited but mitotic slippage is prevented, Bcl-x_L/Bcl-2 phosphorylation levels are also maintained.

CDK-dependent mitotic Bcl-x_L/Bcl-2 phosphorylation. To determine if mitotic Bcl-x_L/Bcl-2 phosphorylation was similarly CDK dependent, KB-3 cells were synchronized by a double thymidine block and, at 7 h postrelease, were treated for 2 h with either the DMSO vehicle, 25 μM Ros, 1 μM PA, or 1 μM RO. As shown in Fig. 8A, each of the CDK inhibitors blocked the increase in Bcl-x_L/Bcl-2 phosphorylation occurring during this interval while maintaining phospho-H3 histone levels. These results suggest that mitotic Bcl-x_L/Bcl-2 phosphorylation is also mediated by a CDK-dependent pathway.

Prolongation of mitosis in the absence of microtubule inhibition is sufficient to induce extensive Bcl-x_L/Bcl-2 phosphorylation. The finding that Bcl-x_L and Bcl-2 are both partially and transiently phosphorylated during mitosis suggests the intriguing possibility that the extensive phosphorylation observed in response to MTIs is due to the prolongation of a CDK-mediated signal initiated in mitosis. To test this hypothesis, we used the proteasome inhibitor MG132 to block cyclin B degradation. Specifically, KB-3 cells were synchronized by the double thymidine block method, and at 10 h postrelease, after mitotic

boundary by a double thymidine block and were treated with 30 nM VBL 1 h after release. Cells were harvested 11 h after release or were incubated for 2 h (i.e., from 11 to 13 h after release) with 25 μM Ros, 1 μM PA, 1 μM RO, or the DMSO vehicle. Immunoblotting for the indicated proteins was performed. Arrows indicate phosphorylated (p) forms. (E) Bcl-x_L phosphorylation is independent of CDK2. Wild-type ($CDK2^{+/+}$) or $CDK2^{-/-}$ primary mouse embryonic fibroblasts were either left untreated (CON) or treated with 30 nM VBL for 8 h. Whole-cell extracts were prepared and immunoblotted for the indicated proteins. The molecular mass of CDK2 is 33 kDa. p-Bcl-x_L, phosphorylated Bcl-x_L. GAPDH was used as a loading control. (F) Inhibition of aurora kinase activity does not alter vinblastine-induced phosphorylation of Bcl-x_L. KB-3 cells were synchronized at the G_1/S boundary by a double thymidine block. Cells were either left untreated or were treated with 30 nM VBL 1 h after release. Nine hours after release, cells were either left untreated or treated with the aurora kinase inhibitor ZM44739 (1 μM). Cells subjected to all four conditions were harvested at 16 h postrelease, and whole-cell extracts were prepared and immunoblotted for the indicated proteins. pH1, phospho-H1 histone; pH3, phospho-H3 histone (Ser10). GAPDH served as a loading control.

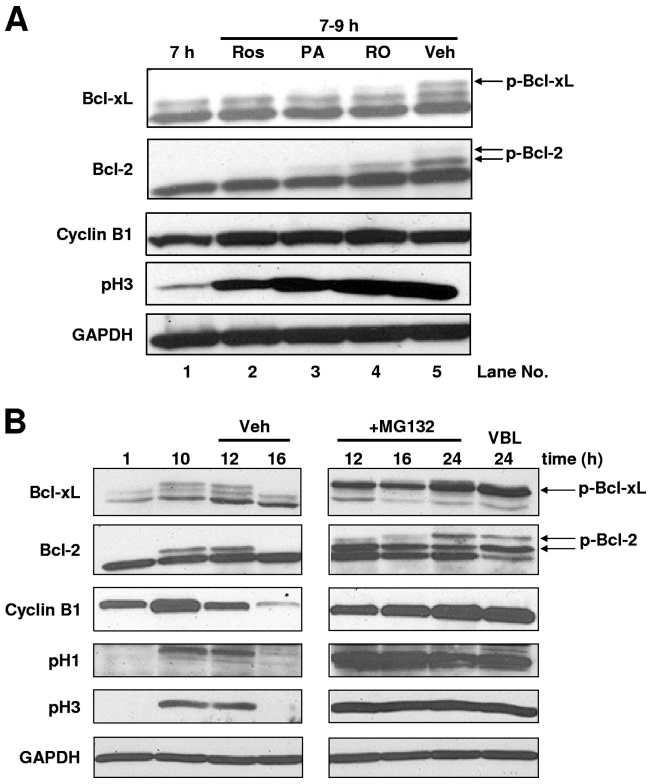

FIG. 8. CDK inhibitors inhibit mitotic Bcl-x_L/Bcl-2 phosphorylation, which is normally transient but is sustained if mitosis is prolonged. (A) Inhibition of CDK inhibits mitotic Bcl-x_L/Bcl-2 phosphorylation. KB-3 cells were synchronized at the G_1/S boundary by a double thymidine block, and at 7 h after release, they were either harvested or treated for 2 h with 25 μM Ros, 1 μM PA, 1 μM RO, or the DMSO vehicle (Veh). Whole-cell extracts were prepared and immunoblotted for the indicated proteins. Arrows indicate phosphorylated (p) forms of Bcl-x_L or Bcl-2. GAPDH was used as a loading control. (B) Prolongation of mitosis without microtubule inhibition leads to sustained Bcl-x_L/Bcl-2 phosphorylation. KB-3 cells were synchronized at the G_1/S boundary by a double thymidine block and were released into complete medium. Two flasks of cells were left untreated and were harvested at 1 h and 10 h postrelease as controls. Other flasks of cells were treated with the DMSO vehicle or with MG132 (20 μM) at 10 h postrelease and were harvested at the indicated time points following release. Whole-cell extracts were prepared and immunoblotted for the indicated proteins. One flask of synchronized cells was treated with 30 nM vinblastine (VBL) for 24 h as a positive control for sustained mitotic arrest. Arrows indicate phosphorylated (p) forms of Bcl-x_L or Bcl-2. GAPDH was used as a loading control.

phosphorylation was initiated but before dephosphorylation had occurred (Fig. 4C), cells were treated with either the vehicle or MG132 (Fig. 8B). In vehicle-treated cells, partial and transient phosphorylation of Bcl-x_L and Bcl-2 was observed, in concert with transient increases in cyclin B1, phospho-H1, and phospho-H3 levels. In MG132-treated cells, in contrast, much more extensive phosphorylation of Bcl-x_L and Bcl-2 was observed, in parallel with sustained accumulation of cyclin B and sustained phosphorylation of H1 and H3 histones. Indeed, the levels of phosphorylation of Bcl-x_L and Bcl-2 observed when mitosis was prolonged by MG132 in this manner approached those observed after treatment with vinblastine (Fig. 8B, far right lane). Thus, in the absence of microtubule inhibition, prolongation of mitosis is sufficient to drive the phosphorylation of Bcl-x_L/Bcl-2 to high levels.

***In vitro* phosphorylation of full-length Bcl-x_L by CDK1.** The results presented above show that CDK1 can directly phosphorylate Ser62 in the context of the peptide substrate FL62 *in vitro* and that mitotic and vinblastine-induced Bcl-x_L/Bcl-2 phosphorylation *in vivo* occurs in a CDK1-dependent manner. However, it remains possible that CDK1 fortuitously phosphorylates FL62 and that a CDK-activated kinase acts as an intermediate to phosphorylate Bcl-x_L/Bcl-2 *in vivo*. To distinguish between these possibilities, we tested whether full-length Bcl-x_L acted as a direct CDK substrate. Recombinant His–Bcl-x_L–ΔC, which has an N-terminal histidine tag and lacks the C-terminal transmembrane domain to enhance solubility, was incubated with increasing amounts of CDK1 in the presence of [γ-^{32}P]ATP. Analysis of ^{32}P incorporation showed that His–Bcl-x_L–ΔC was phosphorylated by CDK1 in a dose-dependent manner (Fig. 9A). The reaction was replicated with nonradioactive ATP in the presence or absence of CDK1 for an extended incubation time of 5 h, and the protein was then excised from SDS gels (Fig. 9B) and analyzed by mass spectrometry after AspN digestion. In the covered sequence (51%), phosphorylation was detected only on Ser62 (Fig. 9C) and was undetectable in control reactions without CDK1 (data not shown). No phosphorylation of Thr47, another potential CDK site within the covered sequence, was observed. Thus, CDK1 directly phosphorylates full-length Bcl-x_L on the physiologically relevant site, Ser62.

Mitochondrial localization of CDK1/cyclin B. In order to extensively phosphorylate Bcl-x_L and Bcl-2 during mitotic arrest, CDK1 would be predicted to localize or translocate to the mitochondria, where these proteins are predominately located (9), after vinblastine treatment. Subcellular fractionation and immunofluorescent microscopy were used to test this prediction. Mitochondria were prepared and purified by sucrose density sedimentation and were subjected to *in vitro* phosphorylation in the absence or presence of FL62. Analysis of the samples by peptide-PAGE showed FL62 kinase activity in mitochondria from vinblastine-treated but not control cells (Fig. 10A). Quantitation of phosphate incorporation into FL62 by the phosphocellulose paper binding method was also performed. The results demonstrated an increase of 3.6-fold in phosphate incorporation in the presence versus the absence of FL62 in the reaction mixtures (Fig. 10B). Caspase-3 and enzymes from the oxidative phosphorylation (OX-PHOS) complex were used as cytosolic and mitochondrial markers, respectively, to show the lack of cross-contamination in the subcellular fractions (Fig. 10C).

Immunofluorescence microscopy (Fig. 10D) revealed that in control cells, CDK1 (green signal) was mainly coincident with nuclei (blue signal) (DAPI) and was distinct in location from the mitochondria (red signal). In vinblastine-treated cells, in contrast, a more diffuse pattern of CDK1 localization was observed: extranuclear staining, some of which coincided with the red mitochondrial signal, was evident. Localization of CDK1 to mitochondria was particularly evident in vinblastine-treated cells displaying condensed chromatin, i.e., mitotically arrested cells, as observed by DAPI staining (Fig. 10D, lower right panels, arrows). Examination of cyclin B by immunofluorescence microscopy revealed elevated levels after vinblastine

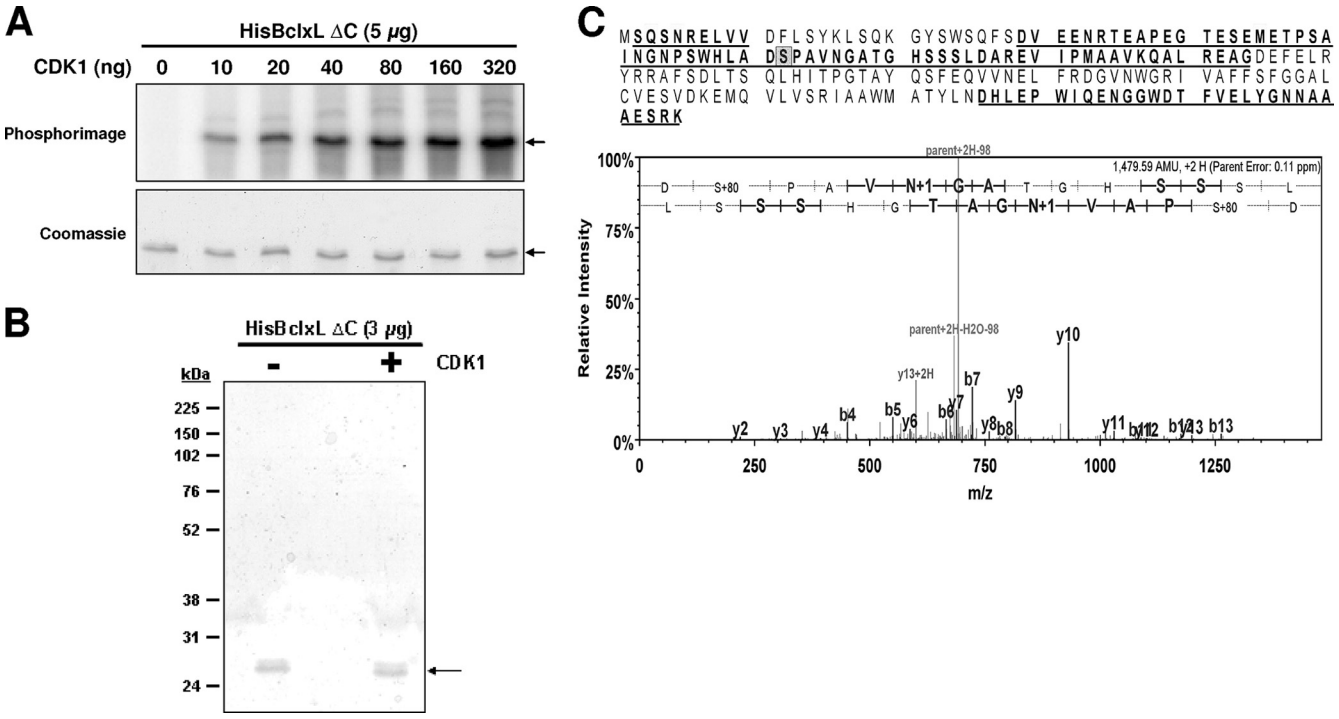

FIG. 9. CDK1 phosphorylates full-length Bcl-x_L on Ser62 *in vitro*. (A) CDK1 phosphorylation of full-length Bcl-x_L. His–Bcl-x_L–ΔC (5 μg) was incubated with 0 to 320 ng of purified, active CDK1/cyclin A2 in a kinase reaction mixture with [γ-^{32}P]ATP, and reaction products were subjected to SDS-PAGE, Coomassie blue staining, and phosphorimager analysis. Arrows indicate His–Bcl-x_L–ΔC. (B) Phosphosite mapping of His–Bcl-x_L phosphorylated by CDK1. His–Bcl-x_L–ΔC (5 μg) was incubated without or with CDK1/cyclin A2 (100 ng) for 5 h at 30°C in a kinase reaction mixture with nonradioactive ATP. Reaction products were subjected to SDS-PAGE and Coomassie staining. His–Bcl-x_L–ΔC is indicated by an arrow, and the positions of molecular size markers are shown. (C) CDK1 phosphorylates Bcl-x_L on Ser62. The bands from each lane in panel B were excised and digested with protease AspN, and peptides were analyzed by electrospray interface LTQ XL-Orbitrap mass spectrometry, as described in Materials and Methods. The covered sequence (51%) is underlined and in boldface. Ser62 is shaded. A representative spectrum from His–Bcl-x_L–ΔC incubated with CDK1 shows the single phosphopeptide detected, DpSPAVNGATGHSSL, on Ser62 (S+80, indicating a molecular mass gain of 80 Da). Phosphorylation was not detected for His–Bcl-x_L–ΔC from the control reaction. N+1 indicates deamidation of Asn-66.

treatment, which in part colocalized with mitochondria, particularly in cells with condensed nuclei (Fig. 10E). Thus, CDK1/cyclin B complexes localize to the mitochondria in cells undergoing mitotic arrest.

Phosphodefective Bcl-x_L blocks cell death induced by nondegradable cyclin B1. To directly test the hypothesis that Bcl-x_L is a key target of proapoptotic CDK1 signaling, KB-3 cells were transiently transfected with a plasmid encoding nondegradable cyclin B1 [cyclin B1(R42A)-GFP]. Plasmids encoding green fluorescent protein (GFP) or wild-type cyclin B1-GFP were used as controls. Fluorescent microscopy 24 h posttransfection demonstrated 50 to 60% transfection efficiency (data not shown), and immunoblotting showed elevated cyclin B1 expression after 24 h (Fig. 11A), which was maintained up to 48 h (data not shown). Apoptotic assays conducted 48 h posttransfection showed that cyclin B1(R42A)-GFP strongly induced cell death, as did wild-type cyclin B1 to a lesser extent, and this was independently confirmed by analysis of PARP cleavage (Fig. 11A). Next, cells were cotransfected with cyclin B1(R42A)-GFP together with either wild-type, phosphodefective (S62A), or phosphomimetic (S62D) HA–Bcl-x_L. Comparable expression of the Bcl-x_L constructs was demonstrated by immunoblotting for the hemagglutinin (HA) tag (Fig. 11B). Cyclin B1(R42A)-GFP-induced apoptotic cell death was strongly inhibited by S62A-Bcl-x_L expression ($P \leq 0.001$ for comparison to wild-type Bcl-x_L), whereas expression of S62D-Bcl-x_L failed to protect cells ($P \leq 0.422$ [not significantly different from wild-type Bcl-x_L]) (Fig. 11B). These results were independently confirmed by analysis of PARP cleavage (Fig. 11B). The data of Fig. 11 provide strong evidence that Bcl-x_L acts as a key substrate for CDK1 proapoptotic signaling.

DISCUSSION

Extensive phosphorylation of Bcl-x_L and Bcl-2 occurs in association with mitotic arrest across a broad spectrum of cell types, and evidence suggests that phosphorylation disables their antiapoptotic function (2, 33, 36). Given the key role of these modifications in regulating the apoptotic death of mitotically arrested cells, and given the need for illumination of the molecular and functional connections between mitotic arrest and apoptosis, identification of the responsible kinase is of obvious significance. However, while several candidates have been proposed (see the introduction), much of the evidence has been indirect and correlative, and no studies of isolation or characterization of the kinase have been reported. By developing and validating a specific assay to enable enzyme characterization, we present evidence here that CDK1/cyclin B is the

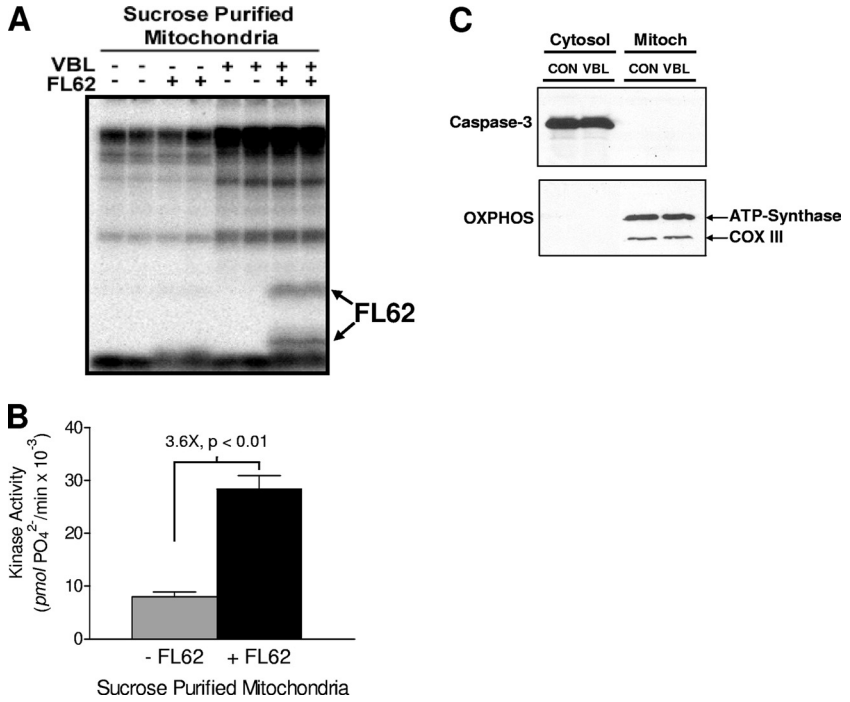

FIG. 10. FL62 kinase localizes to the mitochondria after vinblastine (VBL) treatment. (A) KB-3 cells were either left untreated or treated with 30 nM VBL for 16 h. Mitochondrial fractions were prepared by sucrose density centrifugation and were incubated without or with FL62 in a radioactive kinase reaction mixture in duplicate. Reaction products were subjected to peptide-PAGE and phosphorimager analysis, with a 24-h exposure. The higher- and lower-molecular-weight forms of phosphorylated FL62 are indicated. (B) FL62 kinase activity in purified mitochondria from vinblastine-treated cells. Assays were conducted in triplicate, and ^{32}P incorporation was determined by the P81 filter assay. Results are shown as means ± standard deviations with the *P* value. (C) Cytosolic and mitochondrial molecular markers. Cytosolic and mitochondrial fractions from the control (CON) and VBL-treated samples in panel A were immunoblotted for the cytosolic marker caspase-3 and the indicated mitochondrial markers from the OX-PHOS complex of enzymes, ATP synthase and complex III (COX III). (D) Subcellular localization of CDK1 by immunofluorescence. KB-3 cells were either left untreated (control) or treated with 30 nM vinblastine for 16 h. The cells were costained either with Mitotracker (red), with a polyclonal anti-CDK1 antibody followed by a goat anti-mouse secondary antibody conjugated to FITC (green), or with DAPI (blue). Arrows indicate mitotic cells with condensed chromosomes. (E) Subcellular localization of cyclin B. KB-3 cells were either left untreated (control) or treated with 30 nM vinblastine for 16 h. The cells were costained either with Mitotracker (red), with a monoclonal anti-cyclin B antibody followed by a goat anti-mouse secondary antibody conjugated to FITC (green), or with DAPI (blue). Arrows indicate mitotic cells with condensed chromosomes.

kinase responsible for the extensive phosphorylation of Bcl-x_L and Bcl-2 that occurs in mitotically arrested cells.

Data in support of this conclusion were derived from several experimental approaches. First, as demonstrated by Cks-1 depletion, FL62 kinase activity was clearly due to CDK activity. Evidence that FL62 kinase was CDK1/cyclin B, and not another CDK complex, was provided by the temporal and quantitative characteristics of its activation, which closely matched those of CDK1/cyclin B, both during mitosis and during mitotic arrest (Fig. 3, 4, 6, and 8). In turn, the characteristics of mitotic and MTI-induced Bcl-x_L and Bcl-2 phosphorylation closely matched those of CDK1/cyclin B activity and failed to correlate with the activation of other CDK complexes, including CDK1/cyclin A. Second, validated CDK inhibitors inhibited both mitotic and MTI-induced Bcl-x_L/Bcl-2 phosphorylation. Importantly, the CDK inhibitors demonstrated selectivity, in that they did not directly inhibit the phosphorylation of non-CDK substrates such as histone H3, and further, other kinase inhibitors, including the JNK inhibitor SP600125 (9) and the aurora kinase inhibitor ZM447439 (Fig. 7F), had no effect on MTI-induced Bcl-x_L/Bcl-2 phosphorylation. In addition, vinblastine induced similar levels of Bcl-x_L phosphorylation in both $CDK2^{+/+}$ and $CDK2^{-/-}$ MEFs. Finally, both FL62 and full-length Bcl-x_L acted as substrates for purified CDK1, and Bcl-x_L was specifically phosphorylated on the physiologically relevant site, Ser62, suggesting that CDK1 directly phosphorylates antiapoptotic Bcl-2 proteins. More-recent work from our laboratory has indicated that the antiapoptotic Bcl-2 member Mcl-1 also undergoes CDK1-mediated phosphorylation upon MTI treatment, resulting in Mcl-1 degradation (R. Chu and T. C. Chambers, unpublished data). Thus, CDK1 may be involved in the inactivation of all major Bcl-2 family antiapoptotic proteins during mitotic-arrest-induced apoptosis.

This conclusion contrasts with the suggestions of previous reports that JNK is responsible for MTI-mediated Bcl-x_L or Bcl-2 phosphorylation (2, 11, 36). However, data implicating JNK may be subject to misinterpretation because JNK inhibitors cause cell cycle delay. In carefully controlled experiments using synchronized cells, we have shown that inhibition of JNK profoundly delays the onset of an MTI-induced mitotic block and the corresponding Bcl-x_L/Bcl-2 phosphorylation that occurs (9). Thus, coadministration of both a microtubule inhibitor and a JNK inhibition incorrectly gives the appearance of inhibition of Bcl-x/Bcl-2 phosphorylation, when what is actually

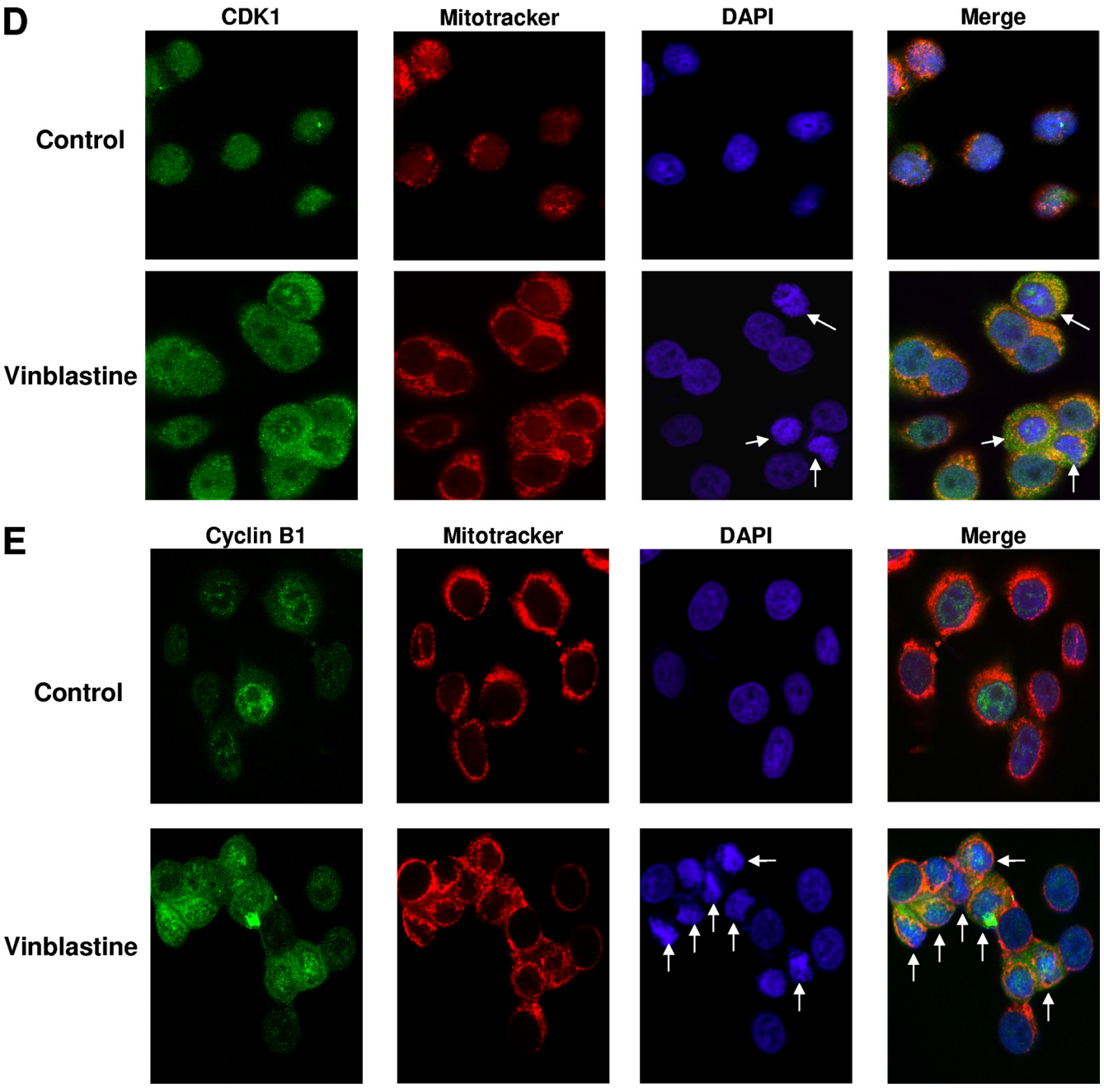

FIG. 10—*Continued.*

being observed is delay of phosphorylation. Indeed, validated inhibition of JNK has no effect on the extent of phosphorylation of these proteins (9). In support of this, JNK failed to phosphorylate the peptide substrate FL62 derived from the known *in vivo* site of phosphorylation in Bcl-x_L, and FL62 kinase was clearly distinct from JNK isozymes based on chromatographic and Cks-1 interaction properties (Fig. 5). Thus, despite the facts that JNK is strongly activated by MTIs and the sites of phosphorylation are proline directed, the evidence presented here argues against JNK being responsible for MTI-induced phosphorylation of these proteins.

A previous report showed that the CDK inhibitor flavopiridol inhibited Taxol-induced Bcl-2 phosphorylation (24). Because cells were cotreated with Taxol and flavopiridol, it remained unclear whether the inhibitory effect of flavopiridol was an indirect consequence of cell cycle suppression. We reported previously that the CDK inhibitor roscovitine failed to appreciably inhibit vinblastine-induced Bcl-x_L/Bcl-2 phosphorylation (9). In that study, roscovitine was added to vinblastine-treated synchronized KB-3 cells for 2 h at 12 h postrelease. Entirely consistent with those results, we found in this study that if roscovitine was added late, at 12 to 14 h, when phosphorylation had nearly reached a peak, it did not display strong inhibitory activity (Fig. 7B). Roscovitine was most ef-

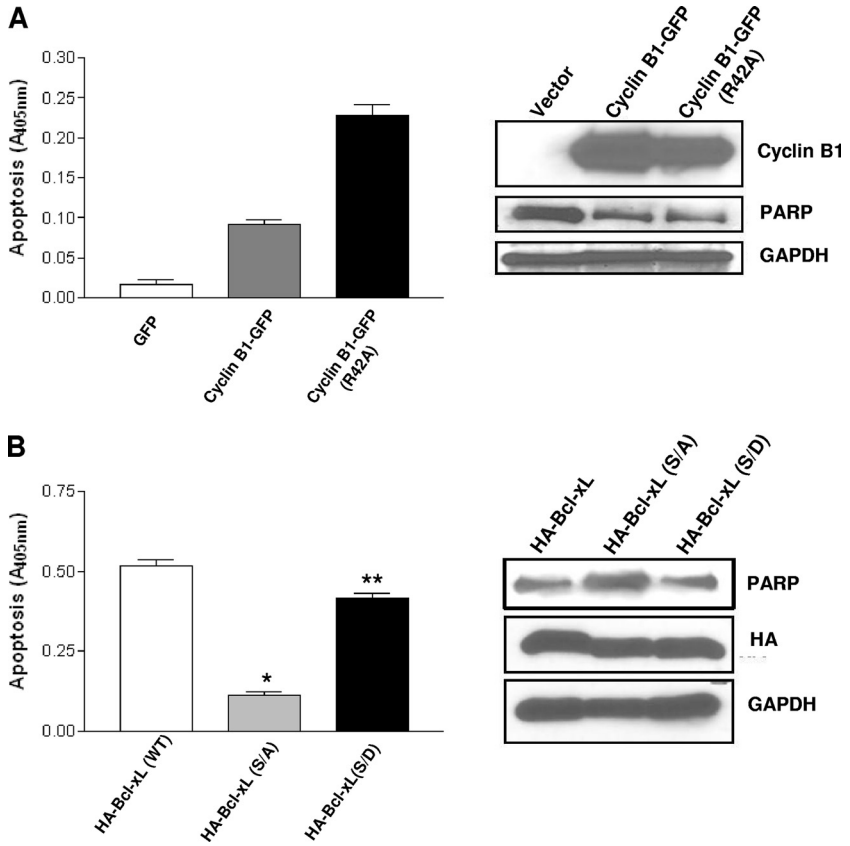

FIG. 11. Phosphodefective Bcl-x_L blocks cell death induced by nondegradable cyclin B1. (A) KB-3 cells were transfected with 1 μg plasmid DNA carrying a GFP vector or encoding wild-type cyclin B1-GFP or cyclin B1(R42A)-GFP. (Left) At 48 h posttransfection, cells were subjected to an apoptotic cell death ELISA. Results are means ± standard deviations ($n = 6$). (Right) Extracts were made and subjected to immunoblotting for cyclin B1 (24 h posttransfection), PARP (48 h posttransfection), or GAPDH. (B) KB-3 cells were transfected with 1 μg plasmid DNA encoding cyclin B1(R42A)-GFP together with 1 μg plasmid DNA encoding either wild-type (WT), phosphodefective (S62A), or phosphomimetic (S62D) HA–Bcl-x_L. (Left) At 48 h posttransfection, cells were subjected to an apoptotic cell death ELISA. Results are means ± standard deviations ($n = 6$). *, $P \leq 0.001$ versus wild-type Bcl-x_L; **, $P \leq 0.422$ versus wild-type Bcl-x_L. (Right) Extracts were made and subjected to immunoblotting for PARP (48 h posttransfection), the HA tag (48 h posttransfection), or GAPDH.

fective when added at earlier time points, corresponding to the rise in Bcl-x_L/Bcl-2 phosphorylation (Fig. 7B and D). Indeed, the experimental design shown in Fig. 7A, with multiple inhibitors used at optimal concentrations at several intervals, was critical in guiding the appropriate conditions for timely CDK1 inhibition, which in turn enabled the generation of more conclusive results.

Both Bcl-x_L and Bcl-2 are subject to partial and transient CDK1-mediated phosphorylation during normal mitotic progression (Fig. 4, 8). While mitotic Bcl-2 phosphorylation has been described for several other cell lines (12, 28), the data presented here are the first, to our knowledge, to show mitotic Bcl-x_L phosphorylation. The fact that these proteins undergo phosphorylation during normal mitosis may explain why microtubule inhibitors are unique among apoptotic stimuli in promoting phosphorylation. By treating mitotic cells with MG132 and blocking mitotic exit, Bcl-x_L/Bcl-2 phosphorylation was dramatically altered, from transient and incomplete to sustained and complete, approaching levels seen in MTI-treated cells (Fig. 8B). These results provide evidence that partial phosphorylation during mitosis is a direct consequence of the transient nature of CDK1 activation, with the loss of CDK1 activity at mitotic exit representing a kinetic limitation on the extent of phosphorylation. Clearly, the low level of phosphorylation that is rapidly reversed as cells reenter G_1 phase is compatible with continued cell survival, whereas the high level of phosphorylation through sustained CDK1 activation during mitotic arrest, lasting 16 to 20 h (9), is associated with an apoptotic outcome. Based on these observations, it is tempting to speculate that the degree of phosphorylation of Bcl-x_L and Bcl-2 may be part of a surveillance mechanism that acts as a readout for the duration of CDK1 activity. Thus, if CDK1 is active transiently, the phosphorylation of Bcl-x_L and Bcl-2 necessarily fails to reach a critical threshold, whereas if the kinase is active for too long, the threshold is breached, driving phosphorylation beyond a level compatible with cell survival, causing inactivation of antiapoptotic function and eventual apoptosis. Such a regulatory system, with different fates stemming from the duration of kinase activation, is not without precedent. JNK, for example, has been shown to have either prosurvival or proapoptotic properties depending on whether the enzyme is active transiently or in a sustained manner (7). Extracellular signal-regulated kinase (ERK) is another example: sustained activation of ERK leads to S-phase

entry of fibroblasts or differentiation of PC12 cells, whereas transient ERK activation fails to elicit these effects (18). The transcription factor c-Fos has been shown to act as a sensor for ERK signal duration (21). Our results suggest the novel possibility that Bcl-x_L and Bcl-2 act as sensors during mitosis for the interpretation of CDK1 signal duration.

The role of CDK1 in M-phase progression is well established, but the role of prolonged CDK1 activity occurring in response to sustained activation of the spindle checkpoint is more controversial (5). The results of certain studies suggest that sustained CDK1 activity plays a proapoptotic role. For example, CDK1 inhibitors have been shown to block Taxol-induced cell death in several cell systems (6, 29, 38). Because studies with phosphodefective mutants of Bcl-x_L and Bcl-2 have consistently suggested that phosphorylation inactivates their antiapoptotic function (33, 36), our results are consistent with sustained CDK1 activity acting in a proapoptotic manner in this context. In support of this possibility, apoptosis induced by nondegradable cyclin B1 was strongly suppressed by cotransfection with phosphodefective Bcl-x_L but was not suppressed by phosphomimetic Bcl-x_L (Fig. 11). Thus, Bcl-x_L acts as a key substrate for proapoptotic CDK1 signaling. However, a cytoprotective role for CDK1 during mitotic arrest, through phosphorylation of survivin (23) or caspase-9 (1), has also been reported. Survivin and caspase-9 operate at the most distal stage of intrinsic apoptosis, whereas Bcl-2 proteins act upstream as regulators. Taken together, the data suggest the intriguing possibility that CDK1 acts as a positive regulator of the preparatory phase of mitotic-arrest-induced apoptosis but as a negative regulator of the execution phase. The existence of such opposing mechanisms may help explain the differing outcomes produced when CDK inhibitors and MTIs are combined (5).

In conclusion, we have provided strong experimental evidence that CDK1/cyclin B is responsible for mitotic and MTI-induced Bcl-x_L and Bcl-2 phosphorylation. The mechanism invoked by these studies, with sustained CDK1 activity catalyzing direct phosphorylation of antiapoptotic Bcl-2 proteins, provides a functional link coupling mitotic arrest and apoptosis. Further, we propose that these key proteins act as sensors for the interpretation of CDK1 signal duration.

ACKNOWLEDGMENTS

We thank D. R. Green for kindly providing the pET29b-BclxL-ΔC plasmid, P. Kaldis for kindly providing mouse embryonic fibroblasts, J. Pines and T. A. Potapova for kindly providing cyclin B1-GFP plasmids, and G. Baldini, S. Mackintosh, R. Kurten, P. Price, and G. Gorbsky for helpful discussions and technical assistance.

This work was supported by Public Health Service grant CA-109821 from the National Cancer Institute (T.C.C.), by pilot study funds from the UAMS College of Medicine Research Council (T.C.C.), by Department of Defense Breast Cancer Program Predoctoral Fellowship Award BC083287 (D.T.T.), and by an American Cancer Society, Illinois Division, Postdoctoral Fellowship (M.U.).

Any opinions, findings, conclusions, or recommendations expressed in this publication are those of the author(s) and do not necessarily reflect the views of the Department of Defense Breast Cancer Program.

REFERENCES

1. **Allan, L. A., and P. R. Clarke.** 2007. Phosphorylation of caspase-9 by CDK1/cyclin B1 protects mitotic cells against apoptosis. Mol. Cell **26:**301–310.
2. **Basu, A., and S. Haldar.** 2003. Identification of a novel Bcl-x_L phosphorylation site regulating the sensitivity of taxol- or 2-methoxyestradiol-induced apoptosis. FEBS Lett. **538:**41–47.
3. **Blagosklonny, M. V., P. Giannakakou, W. S. El-Deiry, D. G. Kingston, P. I. Higgs, L. Neckers, and T. Fojo.** 1997. Raf-1/bcl-2 phosphorylation: a step from microtubule damage to cell death. Cancer Res. **57:**130–135.
4. **Calastretti, A., A. Bevilacqua, C. Ceriani, S. Vigano, P. Zancai, S. Capaccioli, and A. Nicolin.** 2001. Damaged microtubules can inactivate BCL-2 by means of the mTOR kinase. Oncogene **20:**6172–6180.
5. **Castedo, M., J. L. Perfettini, T. Roumier, and G. Kroemer.** 2002. Cyclin-dependent kinase-1: linking apoptosis to cell cycle and mitotic catastrophe. Cell Death Differ. **9:**1287–1293.
6. **Chan, Y. W., H. T. Ma, W. Wong, C. C. Ho, K. F. On, and R. Y. Poon.** 2008. CDK1 inhibitors antagonize the immediate apoptosis triggered by spindle disruption but promote apoptosis following the subsequent rereplication and abnormal mitosis. Cell Cycle **7:**1449–1461.
7. **Davis, R. J.** 2000. Signal transduction by the JNK group of MAP kinases. Cell **103:**239–252.
8. **Desagher, S., A. Osen-Sand, A. Nichols, R. Eskes, S. Montessuit, S. Lauper, K. Maundrell, B. Antonsson, and J. C. Martinou.** 1999. Bid-induced conformational change of Bax is responsible for mitochondrial cytochrome c release during apoptosis. J. Cell Biol. **144:**891–901.
9. **Du, L., C. S. Lyle, and T. C. Chambers.** 2005. Characterization of vinblastine-induced Bcl-x_L and Bcl-2 phosphorylation: evidence for a novel protein kinase and a coordinated phosphorylation/dephosphorylation cycle associated with apoptosis induction. Oncogene **24:**107–117.
10. **Fan, M., L. Du, A. A. Stone, K. M. Gilbert, and T. C. Chambers.** 2000. Modulation of mitogen-activated protein kinases and phosphorylation of Bcl-2 by vinblastine represent persistent forms of normal fluctuations at G_2-M. Cancer Res. **60:**6403–6407.
11. **Fan, M., M. Goodwin, T. Vu, C. Brantley-Finley, W. A. Gaarde, and T. C. Chambers.** 2000. Vinblastine-induced phosphorylation of Bcl-2 and Bcl-x_L is mediated by JNK and occurs in parallel with inactivation of the Raf-1/MEK/ERK cascade. J. Biol. Chem. **275:**29980–29985.
12. **Furukawa, Y., S. Iwase, J. Kikuchi, Y. Terui, M. Nakamura, H. Yamada, Y. Kano, and M. Matsuda.** 2000. Phosphorylation of Bcl-2 protein by CDC2 kinase during G_2/M phases and its role in cell cycle regulation. J. Biol. Chem. **275:**21661–21667.
13. **Haldar, S., N. Jena, and C. M. Croce.** 1995. Inactivation of Bcl-2 by phosphorylation. Proc. Natl. Acad. Sci. U. S. A. **92:**4507–4511.
14. **Harper, J. W.** 2001. Protein destruction: adapting roles for Cks proteins. Curr. Biol. **11:**R431–R435.
15. **Hsu, J. Y., Z. W. Sun, X. Li, M. Reuben, K. Tatchell, D. K. Bishop, J. M. Grushcow, C. J. Brame, J. A. Caldwell, D. F. Hunt, R. Lin, M. M. Smith, and C. D. Allis.** 2000. Mitotic phosphorylation of histone H3 is governed by Ipl1/aurora kinase and Glc7/PP1 phosphatase in budding yeast and nematodes. Cell **102:**279–291.
16. **Kastan, M. B., and J. Bartek.** 2004. Cell-cycle checkpoints and cancer. Nature **432:**316–323.
17. **Letai, A. G.** 2008. Diagnosing and exploiting cancer's addiction to blocks in apoptosis. Nat. Rev. Cancer **8:**121–132.
18. **Marshall, C. J.** 1995. Specificity of receptor tyrosine kinase signaling: transient versus sustained extracellular signal-regulated kinase activation. Cell **80:**179–185.
19. **Meijer, L., A. Borgne, O. Mulner, J. P. Chong, J. J. Blow, N. Inagaki, M. Inagaki, J. G. Delcros, and J. P. Moulinoux.** 1997. Biochemical and cellular effects of roscovitine, a potent and selective inhibitor of the cyclin-dependent kinases cdc2, cdk2 and cdk5. Eur. J. Biochem. **243:**527–536.
20. **Mollinedo, F., and C. Gajate.** 2003. Microtubules, microtubule-interfering agents and apoptosis. Apoptosis **8:**413–450.
21. **Murphy, L. O., S. Smith, R. H. Chen, D. C. Fingar, and J. Blenis.** 2002. Molecular interpretation of ERK signal duration by immediate early gene products. Nat. Cell Biol. **4:**556–564.
22. **Musacchio, A., and E. D. Salmon.** 2007. The spindle-assembly checkpoint in space and time. Nat. Rev. Mol. Cell Biol. **8:**379–393.
23. **O'Connor, D. S., N. R. Wall, A. C. Porter, and D. C. Altieri.** 2002. A p34(cdc2) survival checkpoint in cancer. Cancer Cell **2:**43–54.
24. **Pathan, N., C. Aime-Sempe, S. Kitada, S. Haldar, and J. C. Reed.** 2001. Microtubule-targeting drugs induce Bcl-2 phosphorylation and association with Pin1. Neoplasia **3:**70–79.
25. **Poruchynsky, M. S., E. E. Wang, C. M. Rudin, M. V. Blagosklonny, and T. Fojo.** 1998. Bcl-x_L is phosphorylated in malignant cells following microtubule disruption. Cancer Res. **58:**3331–3338.
26. **Rieder, C. L., and H. Maiato.** 2004. Stuck in division or passing through: what happens when cells cannot satisfy the spindle assembly checkpoint. Dev. Cell **7:**637–651.
27. **Rosania, G. R., J. Merlie, Jr., N. Gray, Y. T. Chang, P. G. Schultz, and R. Heald.** 1999. A cyclin-dependent kinase inhibitor inducing cancer cell differentiation: biochemical identification using Xenopus egg extracts. Proc. Natl. Acad. Sci. U. S. A. **96:**4797–4802.
28. **Scatena, C. D., Z. A. Stewart, D. Mays, L. J. Tang, C. J. Keefer, S. D. Leach, and J. A. Pietenpol.** 1998. Mitotic phosphorylation of Bcl-2 during normal

cell cycle progression and Taxol-induced growth arrest. J. Biol. Chem. **273:** 30777–30784.
29. **Shen, S. C., T. S. Huang, S. H. Jee, and M. L. Kuo.** 1998. Taxol-induced p34cdc2 kinase activation and apoptosis inhibited by 12-O-tetradecanoylphorbol-13-acetate in human breast MCF-7 carcinoma cells. Cell Growth Differ. **9:**23–29.
30. **Skoufias, D. A., R. L. Indorato, F. Lacroix, A. Panopoulos, and R. L. Margolis.** 2007. Mitosis persists in the absence of Cdk1 activity when proteolysis or protein phosphatase activity is suppressed. J. Cell Biol. **179:**671–685.
31. **Sorger, P. K., M. Dobles, R. Tournebize, and A. A. Hyman.** 1997. Coupling cell division and cell death to microtubule dynamics. Curr. Opin. Cell Biol. **9:**807–814.
32. **Srivastava, R. K., A. R. Srivastava, S. J. Korsmeyer, M. Nesterova, Y. S. Cho-Chung, and D. L. Longo.** 1998. Involvement of microtubules in the regulation of Bcl2 phosphorylation and apoptosis through cyclic AMP-dependent protein kinase. Mol. Cell. Biol. **18:**3509–3517.
33. **Upreti, M., E. N. Galitovskaya, R. Chu, A. J. Tackett, D. T. Terrano, S. Granell, and T. C. Chambers.** 2008. Identification of the major phosphorylation site in Bcl-x_L induced by microtubule inhibitors and analysis of its functional significance. J. Biol. Chem. **283:**35517–35525.
34. **Vassilev, L. T., C. Tovar, S. Chen, D. Knezevic, X. Zhao, H. Sun, D. C. Heimbrook, and L. Chen.** 2006. Selective small-molecule inhibitor reveals critical mitotic functions of human CDK1. Proc. Natl. Acad. Sci. U. S. A. **103:**10660–10665.
35. **Weaver, B. A., and D. W. Cleveland.** 2005. Decoding the links between mitosis, cancer, and chemotherapy: the mitotic checkpoint, adaptation, and cell death. Cancer Cell **8:**7–12.
36. **Yamamoto, K., H. Ichijo, and S. J. Korsmeyer.** 1999. BCL-2 is phosphorylated and inactivated by an ASK1/Jun N-terminal protein kinase pathway normally activated at G(2)/M. Mol. Cell. Biol. **19:**8469–8478.
37. **Youle, R. J., and A. Strasser.** 2008. The BCL-2 protein family: opposing activities that mediate cell death. Nat. Rev. Mol. Cell Biol. **9:**47–59.
38. **Yu, D., T. Jing, B. Liu, J. Yao, M. Tan, T. J. McDonnell, and M. C. Hung.** 1998. Overexpression of ErbB2 blocks Taxol-induced apoptosis by upregulation of p21Cip1, which inhibits p34Cdc2 kinase. Mol. Cell **2:**581–591.